

1 The *Plasmodium falciparum* rhoptry protein RhopH3
2 plays essential roles in host cell invasion and nutrient
3 uptake

4
5 Emma S. Sherling^{1, 2}, Ellen Knuepfer¹, Joseph A. Brzostowski³, Louis H.
6 Miller², Michael J. Blackman^{1, 4*}, Christiaan van Ooij^{1*}

7
8 ¹The Francis Crick Institute, 1 Midland Road, London, NW1 1AT, United
9 Kingdom

10 ²Laboratory of Malaria and Vector Research and ³Laboratory of
11 Immunogenetics Imaging Facility, National Institute of Allergy and Infectious
12 Disease, National Institute of Health, Rockville, MD 20852, USA

13 ⁴Department of Pathogen Molecular Biology, London School of Hygiene &
14 Tropical Medicine, London WC1E 7HT, United Kingdom

15
16
17
18
19
20
21
22
23
24
25
26
27
28
29
30
31
32
33
34
35
36
37
38
39
40
41
42
43
44 Correspondence and requests for materials should be addressed to M.J.B.
45 (email: Mike.Blackman@crick.ac.uk) or C.v.O. (email:
46 Christiaan.vanOoij@crick.ac.uk)

47
48

49

50

51

52 **Abstract**

53 Merozoites of the protozoan parasite responsible for the most virulent form

54 of malaria, *Plasmodium falciparum*, invade erythrocytes. Invasion involves

55 discharge of rhoptries, specialized secretory organelles. Once intracellular,

56 parasites induce increased nutrient uptake by generating new permeability

57 pathways (NPP) including a *Plasmodium* surface anion channel (PSAC).

58 RhopH1/Clag3, one member of the three-protein RhopH complex, is

59 important for PSAC/NPP activity. However, the roles of the other members

60 of the RhopH complex in PSAC/NPP establishment are unknown and it is

61 unclear whether any of the RhopH proteins play a role in invasion. Here we

62 demonstrate that RhopH3, the smallest component of the complex, is

63 essential for parasite survival. Conditional truncation of RhopH3

64 substantially reduces invasive capacity. Those mutant parasites that do

65 invade are defective in nutrient import and die. Our results identify a dual

66 role for RhopH3 that links erythrocyte invasion to formation of the

67 PSAC/NPP essential for parasite survival within host erythrocytes.

68

69

70 Introduction

71 Parasites of the genus *Plasmodium* are the causative agents of malaria, a
72 disease that claims nearly 600,000 lives each year (1). Of the five
73 *Plasmodium* species that infect humans, *Plasmodium falciparum* is
74 responsible for nearly all the mortality associated with malaria. The disease
75 is the result of asexual replication of the parasite in erythrocytes. For
76 approximately the first half of the 48 h *P. falciparum* intraerythrocytic life
77 cycle, the parasite exists in a mononuclear trophozoite form (the earliest
78 stages of which are generally referred to as ring stages), during which the
79 parasite grows rapidly. During this phase, *P. falciparum*-infected
80 erythrocytes gain the capacity to adhere to host vascular endothelium, a
81 process that depends on the export of parasite proteins to form adhesive
82 structures called knobs at the host erythrocyte surface. Nuclear division
83 then commences, initiating differentiation into a schizont (a process called
84 schizogony). This multinucleated form eventually undergoes segmentation
85 to form invasive merozoites that egress upon rupture of the infected
86 erythrocyte to invade new erythrocytes.

87 Egress and erythrocyte invasion involves the regulated discharge of
88 several sets of apical merozoite secretory organelles that are unique to
89 apicomplexan parasites. The largest of these organelles, called rhoptries,
90 contain several proteins involved in adhesion to the host cell. Rhoptries are
91 also thought to mediate formation of the nascent parasitophorous vacuole
92 (PV), a membranous compartment that surrounds the parasite after entry
93 has been completed (2,3). Despite the importance of rhoptries in invasion
94 and subsequent host cell remodeling, a detailed understanding of the

95 function of many rhoptry proteins is lacking. Rhoptries comprise at least two
96 subdomains(3) referred to as the rhoptry neck and the bulb. The contents of
97 these subdomains likely mediate different functions, as reflected by
98 evidence suggesting that they are released sequentially during invasion (4).
99 Proteins of the rhoptry neck are well conserved between *Plasmodium spp.*
100 and the related apicomplexan parasite *Toxoplasma gondii*, suggesting
101 conserved functions (3,5). In contrast, proteins of the rhoptry bulb appear
102 to be genus-specific, perhaps reflecting functions unique to each parasite
103 (3). A function for several *Plasmodium* rhoptry bulb proteins has been
104 proposed, such as a role for a protein called RAMA in transport of proteins
105 to the rhoptry (6), but the inability to produce mutants lacking these
106 proteins has precluded conclusive assignments of function (7). Hence, the
107 molecular functions of most rhoptry proteins remain unknown.

108 One component of the *P. falciparum* rhoptry bulb that has received
109 particular attention is the so-called high molecular weight (HMW) rhoptry or
110 RhopH complex, which consists of three proteins called RhopH1/Clag,
111 RhopH2, and RhopH3 (8,9). Whilst RhopH2 and RhopH3 are each encoded by
112 single-copy genes, RhopH1/Clag, the largest component of the complex,
113 exists in 5 isotypes encoded by separate genes entitled *clag2*, *clag3.1*,
114 *clag3.2*, *clag8* and *clag9* (10,11). RhopH1/Clag3.1 and RhopH1/Clag3.2 are
115 nearly identical proteins that are expressed in a mutually exclusive manner
116 (12-14). Each RhopH complex contains only one form of RhopH1/Clag (11),
117 so each parasite has the potential to produce four different RhopH
118 complexes, differentiated by the particular RhopH1/Clag isotype bound. All
119 members of the RhopH complex are expressed late in the intraerythrocytic

120 cycle (8). The complex is then released during invasion (15) and inserted
121 into the nascent PV membrane (PVM) soon after parasite entry (16,17).

122 Genetic and chemical genetic investigation has revealed a role for
123 the RhopH1/Clag3 proteins in the function of the *Plasmodium* surface anion
124 channel (PSAC), a new permeability pathway (NPP) induced in host
125 erythrocytes following parasite entry and involved in nutrient acquisition by
126 the intracellular parasite (18). Pharmacological inhibition of
127 RhopH1/Clag3.2 function was found to block PSAC/NPP activity, and
128 selection for drug-resistant mutants revealed that part of the protein is
129 exposed at the surface of the erythrocyte and that it may form the channel
130 itself (19,20). However, parasites that do not produce either
131 RhopH1/Clag3.1 or RhopH1/Clag3.2 display only a small growth
132 disadvantage (13) and inhibition of the function of these proteins has only a
133 small effect on parasite growth rates *in vitro* (21). Parasites lacking
134 RhopH1/Clag9 are viable, and an early report suggested that loss of the
135 *clag9* gene resulted in loss of binding to CD36 (22). However, this has been
136 disputed (23), as a subsequent study identified another gene closely linked
137 to the *clag9* gene that is important for CD36 binding (24). Hence, whilst the
138 function of RhopH1/Clag9 remains to be determined, like RhopH1/Clag3.1
139 and RhopH1/Clag 3.2, it is not essential. There are no reports describing a
140 deletion, or attempted deletion, of *clag2* or *clag8*.

141 Much less is known of the function of the RhopH2 and RhopH3
142 components of the complex. There is no report of attempted disruption of
143 the *rhopH2* gene, but the *rhopH3* gene is refractory to deletion in the
144 haploid blood stages (25), suggesting an essential role. Hints that this might

145 include a function in invasion derive from studies showing that antibodies to
146 RhopH3 can inhibit invasion (8,26). However, whether RhopH3 plays other
147 essential roles that involve all forms of the RhopH complex is unknown.

148 Here we use a conditional mutagenesis approach to modify the
149 *rhopH3* gene in a manner that blocks formation of the RhopH complex. The
150 resulting mutant parasites show two distinct phenotypes: a significant
151 decrease in the level of erythrocyte invasion and a complete block in
152 intracellular development at the trophozoite stage. Our findings reveal that
153 RhopH3 and the RhopH complex have essential roles in two distinct stages of
154 the erythrocytic lifecycle.

155

156 **Results**

157 **Efficient conditional truncation of the *rhopH3* gene.** Previous attempts to
158 disrupt the *P. falciparum* *rhopH3* gene using conventional genetic
159 techniques were unsuccessful (25), suggesting an indispensable role in
160 asexual blood stages. To gain insights into this role we therefore adopted
161 the DiCre conditional recombinase system recently adapted to *P. falciparum*
162 (27) to examine the consequences of functional inactivation of RhopH3. For
163 this, we used Cas9-mediated genome editing (28) to introduce synthetic
164 introns containing *loxP* sites (29) into the *rhopH3* gene such that they
165 flanked an internal region spanning exons 4-6, the region of the gene that
166 shows the highest level of conservation across *Plasmodium* *rhopH3* orthologs
167 (Figure 1A, Figure 1 - figure supplement 1). This genomic modification was
168 made in the DiCre-expressing *P. falciparum* 1G5DC parasite clone (27) in
169 order that excision of the floxed sequence could be induced by treatment of

170 the transgenic parasites with rapamycin. DiCre-mediated excision was
171 predicted to generate an internally-truncated mutant form of *rhopH3*
172 lacking its most highly conserved region.

173 Successful modification of the *rhopH3* gene in the transfected
174 parasite population following introduction of the targeting vector was
175 confirmed by diagnostic PCR (not shown). Subsequent limiting dilution
176 cloning of the modified parasites resulted in the isolation of parasite clones
177 *rhopH3-loxP* 5F5 and *rhopH3-loxP* 4B11, which were derived from
178 independent transfections using different guide RNAs. Modification of the
179 native *rhopH3* locus in the expected fashion was confirmed in both parasite
180 clones by diagnostic PCR and Southern blot (Figure 1B and Figure 1C). Both
181 clones displayed RhopH3 expression levels and *in vitro* replication rates
182 indistinguishable from the parental 1G5DC parasites (Figure 1 - figure
183 supplement 2), indicating that the modified *rhopH3* gene generated wild
184 type levels of RhopH3 and that the modifications had no impact on parasite
185 viability. The clones were therefore used for all subsequent experiments.

186 To examine the efficiency of conditional excision of the floxed
187 sequence in the *rhopH3-loxP* clones, tightly synchronized ring stage cultures
188 of both clones were divided into two and treated for 4 h with either
189 rapamycin or DMSO (vehicle control). Following washing and further
190 incubation for ~44 h to allow maturation of the parasites to schizont stage
191 (at which peak expression of RhopH3 occurs (8)), genomic DNA from the
192 clones was examined by PCR and Southern blot. This revealed highly
193 efficient excision of the floxed *rhopH3* sequence (Figure 1D and Figure 1E).

194 DiCre-mediated site-specific recombination between the introduced
195 *loxP* sites in the modified *rhopH3* locus of the *rhopH3-loxP* parasites was
196 expected to reconstitute a functional, albeit chimeric, intron. Upon splicing
197 of this intron exons 3 and 7 are placed in frame, producing a modified
198 RhopH3 gene product (called RhopH3 Δ 4-6) that retains wild type N-terminal
199 and C-terminal segments but lacking residues encoded by exons 4-6.
200 Extracts of the rapamycin-treated and control parasites were analyzed by
201 immunoblot ~44 h following treatment using antibody anti-Ag-44, which
202 recognizes an epitope within the C-terminal segment of RhopH3 encoded by
203 exon 7 (30). As shown in Figure 1F and Figure 1 - figure supplement 3,
204 rapamycin treatment produced the expected change in mass, converting the
205 ~110 kDa wild-type RhopH3 to a ~70 kDa RhopH3 Δ 4-6 product. This
206 conversion was highly efficient, with no residual full-length protein
207 detected in the rapamycin-treated schizonts. These results confirmed the
208 excision data and demonstrated essentially complete conditional truncation
209 of RhopH3 within a single erythrocytic cycle in the *rhopH3-loxP* parasite
210 clones.

211

212 **Truncation of *rhopH3* leads to mislocalization of other components of the**
213 **RhopH complex.** We next aimed to determine the effects of RhopH3
214 truncation on its subcellular localization within the parasite, as well as on
215 the trafficking of other members of the RhopH complex.

216 Immunofluorescence analysis (IFA) showed that, as expected, RhopH3
217 colocalized with the rhoptry marker RAP2 (31,32) in mature schizonts of
218 control *rhopH3-loxP* parasites (Figure 2A). However, in rapamycin-treated

219 (RhopH3 Δ 4-6) parasites, this colocalization was lost, although RAP2 was still
220 detected in a punctate, apically-disposed pattern typical of rhoptries
221 (Figure 2A). To determine the effects of this mistrafficking on localization of
222 the other two RhopH complex proteins, control and rapamycin-treated
223 *rhopH3-loxP* parasites were probed with anti-RAP2 as well as either anti-
224 RhopH1/Clag3.1 (11) or anti-RhopH2 antibodies (9). This showed that, as in
225 the case of RhopH3, rhoptry localization of both RhopH1/Clag3.1 and
226 RhopH2 was lost in rapamycin-treated parasites (Figure 2A). These results
227 indicated that truncation of RhopH3 to the RhopH3 Δ 4-6 form resulted in
228 mistrafficking of at least some components of the RhopH complex. To
229 determine whether the mistrafficked rhoptry proteins all localized to the
230 same parasite compartment, the parasites were co-stained with various
231 combinations of antibodies against two of the three complex proteins. This
232 showed that neither RhopH2 nor RhopH1/Clag3.1 colocalized with
233 RhopH3 Δ 4-6 in the mutant parasites (Figure 2B). The RhopH2 and
234 RhopH1/Clag3.1 signals were also distinct in the mutant parasites, although
235 in this case some limited colocalization of these proteins was apparent
236 (bottom images, Figure 2B).

237 To better define the fate of the mistrafficked RhopH3 Δ 4-6 in the
238 mutant parasites, rapamycin-treated mature schizonts were probed with
239 antibodies to the merozoite plasma membrane surface marker MSP1. This
240 indicated that the mutant protein was expressed in a location surrounding
241 (and so likely external to) the plasma membrane of individual segmented
242 intracellular merozoites (Figure 2 - figure supplement 1). In confirmation of
243 this, IFA of naturally released free merozoites showed that the truncated

244 RhopH3 Δ 4-6 was often largely undetectable in merozoites of the mutant
245 parasites (Figure 2C).

246 One interpretation of these results was that truncation of RhopH3
247 interfered with formation of the RhopH complex. To test this notion, we
248 used a monoclonal antibody (mAb) specific for RhopH2 to
249 immunoprecipitate the complex from extracts of schizonts of *rhopH3-loxP*
250 clone 5F5. As shown in Figure 2D, both RhopH3 and RhopH1/Clag3.1 were
251 precipitated as expected from lysates of control parasites. In contrast,
252 RhopH3 Δ 4-6 was undetectable in the precipitate from lysates of rapamycin-
253 treated parasites, although RhopH1/Clag3.1 could still be detected. This
254 showed that truncation of RhopH3 ablates its association with RhopH2,
255 although it does not appear to affect the interaction between RhopH2 and
256 RhopH1/Clag3.1. Collectively, these results suggested that truncation of
257 RhopH3 caused mistrafficking of other components of the complex, probably
258 due to loss of the association between RhopH3 and these other proteins.

259

260 **Loss of the RhopH complex is a lethal event.** The above results showed
261 that whilst truncation of RhopH3 affected trafficking of the RhopH complex,
262 it did not prevent schizont development in the erythrocytic growth cycle in
263 which the parasites were treated with rapamycin (henceforth referred to as
264 cycle 1). To evaluate the effects of RhopH3 modification and mistrafficking
265 on longer-term parasite viability, we first exploited a recently developed
266 assay in which parasite replication is assessed in 96-well microplates over a
267 period of 5-7 erythrocytic cycles by visualization of the localized lysis of
268 host erythrocytes in static cultures in 96-well microplates. Under these

269 conditions, successful parasite growth results in formation of
270 microscopically discernible zones of clearance of erythrocytes referred to as
271 plaques (33). As shown in Table 1, in 3 separate assays DMSO-treated
272 *rhopH3-loxP* parasites seeded at ~10 parasites per well produced plaques in
273 nearly every well, with a mean average of ~8 plaques per well for clone 5F5
274 and ~5 plaques per well for clone 4B11 (Table 1). In contrast, in the plates
275 seeded with an identical density of rapamycin-treated parasites, only ~10%
276 of the wells contained plaques and no well contained more than one plaque
277 (Figure 3A, Table 1). Analysis by diagnostic PCR of several parasite clones
278 isolated from individual plaques that appeared in plates seeded with
279 rapamycin-treated parasites revealed that in all cases they derived from
280 parasites that possessed an intact *rhopH3-loxP* gene, indicating that these
281 corresponded to a small subpopulation of parasites in which excision of the
282 floxed sequence had not taken place (Figure 3B). Further analysis by PCR of
283 one of these non-excised clones showed that the DiCre cassette had been
284 lost (Figure 3C) probably due to a genomic rearrangement. This parasite
285 clone (named RhopH3 NE) served as a useful control for subsequent
286 experiments.

287 To further examine the effects of RhopH3 truncation on long-term
288 parasite viability, low parasitaemia cultures of the *rhopH3-loxP* clones 5F5
289 and 4B11 were divided equally into two flasks, treated with either DMSO or
290 rapamycin, then the parasites simply maintained in continuous culture,
291 monitoring increase in parasitaemia at 48 h intervals as well taking samples
292 for analysis by diagnostic PCR. Cultures of the parental 1G5DC parasites as
293 well as the DiCre-defective RhopH3 NE clone were similarly treated and

294 monitored in parallel. As shown in Figure 3D, whilst replication of the
295 1G5DC and RhopH3 NE parasites was unaffected by rapamycin treatment,
296 the rapamycin-treated 5F5 and 4B11 clones showed a dramatic decrease in
297 growth rate. However in both clones the appearance of replicating parasites
298 was evident by cycle 3, suggesting that these might correspond to a minor
299 population of normally-replicating non-excised parasites. Diagnostic PCR
300 analysis of the 5F5 culture supported this notion. At the end of cycle 1, PCR
301 using primers that distinguish between the excised and non-excised locus
302 showed the expected highly efficient excision of the floxed *rhopH3-loxP*
303 sequence in the rapamycin-treated culture, with the non-excised locus
304 undetectable. However, periodic examination of the parasites by diagnostic
305 PCR over the ensuing 6 erythrocytic cycles showed a time-dependent
306 increase in the proportion of non-excised parasites in the rapamycin-treated
307 culture, suggesting that the initially undetectable population of non-excised
308 parasites gradually overgrew the cultures. This occurred likely as a result of
309 a selective advantage conferred on them by the replication defect displayed
310 by the RhopH3 Δ 4-6 parasites. By cycle 5, the excised locus was hardly
311 detectable in the rapamycin-treated culture (Figure 3E). Together with the
312 results of the plaque assay, these results allowed us to conclude that
313 truncation of RhopH3 results in complete loss of long-term parasite viability.
314

315 **Loss of the RhopH complex leads to an invasion defect.** The severe growth
316 defect displayed in the plaque and growth assays could result from an
317 inability of mutant parasites to egress from the host erythrocyte, a block in
318 invasion, or a developmental arrest during intracellular growth. We

319 therefore next investigated the capacity of RhopH3 Δ 4-6 parasites to undergo
320 egress. For this, we used time-lapse differential interference contrast (DIC)
321 microscopy to observe the egress of merozoites from highly mature,
322 synchronized schizonts at the end of cycle 1 (i.e. ~45 h following treatment
323 of ring-stage *rhopH3-loxP* parasites with rapamycin or DMSO). This revealed
324 no gross differences in the efficiency or morphology of egress
325 (Supplementary video 1), indicating that the absence of the RhopH complex
326 from rhoptries does not affect egress.

327 To investigate a potential invasion phenotype resulting from RhopH3
328 truncation, a synchronized culture of *rhopH3-loxP* parasites at early ring
329 stage was divided into two, treated with either DMSO or rapamycin and then
330 allowed to mature to schizont stage before purifying the mature schizonts
331 and adding them to fresh erythrocytes. After incubation for a further 4 h to
332 allow the *rhopH3-loxP* schizonts to undergo merozoite egress and invasion,
333 the percentage of erythrocytes infected with cycle 2 ring-stage parasites
334 was quantified. The results consistently showed that the ring-stage
335 parasitemia values in cultures derived from the rapamycin-treated *rhopH3-*
336 *loxP* parasites was only ~50% of that in their DMSO-treated counterparts
337 (Figure 3F). Importantly, invasion by the control RhopH3 NE and the
338 parental 1G5DC parasites was unaffected by rapamycin treatment. Taken
339 together with the other results, these data showed that the absence of the
340 RhopH complex from parasite rhoptries significantly affects the ability of
341 the parasite to invade new host cells.

342

343 The RhopH complex is required for intracellular parasite development.
344 Although the results of the above experiments pointed to a severe invasion
345 defect in parasites lacking the RhopH complex, it was unclear whether this
346 could be sufficient to explain the results of the plaque assay, which
347 indicated a complete lack of long-term viability in the RhopH3 Δ 4-6 mutants.
348 To explore this further, we examined growth and development of the
349 mutants using microscopic examination of Giemsa-stained cultures. This
350 showed that whereas rapamycin-treated *rhopH3-loxP* parasites appeared
351 morphologically normal at the end of the cycle 1 as well as at the ring stage
352 of cycle 2, development of the mutant parasites stalled at trophozoite stage
353 in cycle 2 (Figure 4A) and the parasites did not develop into schizonts. To
354 confirm this developmental block we used flow cytometry to monitor the
355 DNA content of the parasites in cycle 2. This confirmed that rings derived
356 from rapamycin-treated *rhopH3-loxP* parasites did not increase their DNA
357 content during cycle 2 (Figure 4B), i.e. they did not progress to the
358 multinuclear schizont stage. Taken together, these data indicated that the
359 RhopH complex is essential for the trophozoite to schizont developmental
360 transition of the intracellular parasite.

361

362 Protein export occurs normally in the RhopH3 Δ 4-6 mutants. Export of
363 parasite proteins into the host erythrocyte is important for parasite
364 virulence and for the uptake of nutrients; blocking export prevents
365 modification of the erythrocyte surface with the knob structures that play a
366 role in cytoadhesion, and also prevents development of the parasite beyond
367 the trophozoite stage (34,35). Since we observed a similar growth

368 phenotype in cycle 2 in the RhopH3 Δ 4-6 parasites, we decided to determine
369 whether the developmental arrest was the result of a generalized defect in
370 protein export. To do this, we examined the subcellular localization of
371 KAHRP and MAHRP1, parasite proteins that are established markers for
372 protein export and Maurer's clefts (intraerythrocytic membranous structures
373 of parasite origin) respectively, in cycle 2 trophozoites derived from
374 rapamycin-treated *rhopH3-loxP* parasites (36,37). This revealed no
375 discernible alterations in protein export and Maurer's cleft formation in the
376 RhopH3 Δ 4-6 mutants (Figure 5A). This conclusion was corroborated by
377 electron microscopy, which revealed the formation of knobs on the surface
378 of erythrocytes infected with rapamycin-treated *rhopH3-loxP* parasites
379 (Figure 5B). We concluded that protein export from the intracellular
380 parasite can take place normally in the absence of the RhopH complex.

381

382 **Import pathways are defective in *rhopH3* mutant parasites.** The
383 developmental arrest observed in cycle 2 trophozoites of the RhopH3 Δ 4-6
384 parasites was strikingly reminiscent of the effect of isoleucine starvation on
385 *P. falciparum* (38) Isoleucine is transported into the parasitized cell via the
386 PSAC/NPP, the parasite-induced uptake pathway responsible for enhanced
387 nutrient uptake in parasite-infected erythrocytes (39). The PSAC/NPP is also
388 responsible for the permeability of parasite-infected erythrocytes to the
389 alcohol sugar sorbitol (18), leading to the capacity of sorbitol solutions to
390 mediate osmotic lysis of infected erythrocytes. This lysis can be readily
391 quantified by measuring levels of host cell hemoglobin released following
392 treatment of parasitized cells with a sorbitol solution (40). To determine

393 whether the PSAC/NPP was functional in the RhopH3 Δ 4-6 mutants, their
394 resistance to sorbitol-mediated lysis was assessed. As shown in Figure 6A,
395 erythrocytes infected with parental 1G5DC parasites or the non-excised
396 RhopH3 NE clone displayed the expected sensitivity to sorbitol, as did
397 erythrocytes infected with control (DMSO-treated) *rhopH3-loxP* parasites. In
398 contrast, erythrocytes infected with cycle 2 rapamycin-treated *rhopH3-loxP*
399 parasites were insensitive to sorbitol; the amount of hemoglobin released
400 upon sorbitol treatment was not significantly different from the amount
401 released by treatment of the infected erythrocytes with an isotonic control
402 buffer (PBS).

403 To further investigate the activity of the PSAC/NPP in the RhopH3 Δ 4-
404 6 mutants, erythrocytes infected with cycle 2 rings were incubated with 5-
405 aminolevulinic acid (5-ALA). This compound is excluded from uninfected
406 erythrocytes but is taken up by infected erythrocytes and converted to
407 fluorescent protoporphyrin IX (PPIX) (41). Import of 5-ALA has previously
408 been shown to be sensitive to furosemide, a small molecule inhibitor of
409 PSAC/NPP, and is also blocked upon downregulation of parasite export and
410 PSAC/NPP activity in transgenic *P. falciparum* (34,41,42). Import of 5-ALA
411 therefore acts as a convenient reporter for PSAC/NPP activity. Examination
412 by fluorescence microscopy (Figure 6B and 6C) and FACS (Figure 6D) showed
413 that erythrocytes infected with DMSO-treated *rhopH3-loxP* clone 5F5 and
414 4B11 parasites readily took up 5-ALA, whereas no fluorescence was observed
415 in erythrocytes infected with rapamycin-treated *rhopH3-loxP* parasites
416 following incubation with 5-ALA. In contrast, rapamycin-treatment had no
417 effect on the capacity of the parental 1G5DC or DiCre-deficient RhopH3 NE

418 parasites to take up 5-ALA (Figure 6B-D). Combined, these results
419 convincingly indicate that the PSAC/NPP is defective in the *rhopH3* mutants.

420

421 Discussion

422 In this study we have shown that RhopH3 plays a central role in the
423 formation of a functional RhopH complex and that mutation of RhopH3
424 results in two severe, but very distinct, phenotypes: 1) a ~50% decrease in
425 host erythrocyte invasion; and 2) a block in the development in the early
426 trophozoite stage of those parasites that do invade. This block in
427 development is a lethal event; no parasites carrying the mutant form of the
428 *rhopH3-loxP* gene were recovered in a plaque assay and parasites with an
429 intact *rhopH3-loxP* gene quickly outgrew the mutant parasites after
430 rapamycin treatment. These results represent the first published evidence
431 that RhopH3 is essential and mark the first time a rhoptry protein has been
432 shown to have two separate, seemingly unrelated functions at different
433 stages of the erythrocytic life cycle. RhopH3 is also the first rhoptry bulb
434 protein to be directly assigned a role in invasion; other rhoptry proteins
435 previously experimentally implicated in invasion are located in the rhoptry
436 neck. The release of rhoptry neck proteins is considered the step at which
437 the parasite commits to host cell entry (43), so the discovery of an
438 important invasion factor that is presumably released later in the invasion
439 pathway is important.

440 Whilst it was surprising that loss of the function of the RhopH
441 complex leads to two different, seemingly unrelated, phenotypes, previous
442 results had hinted at a role for RhopH3 and the complex in both processes.

443 RhopH3, and proteolytic fragments of RhopH3, can bind to erythrocytes and
444 to liposomes (44,45). This appears to occur even in the absence of other
445 members of the RhopH complex, indicating that, for its role in invasion,
446 RhopH3 may not require the function of the other proteins of the complex.
447 Further supporting a role for RhopH3 in invasion is the finding that anti-
448 RhopH3 antibodies can block invasion (26,45). Nonetheless it is curious that
449 ~50% of the parasites still enter the erythrocyte in the absence of full-length
450 RhopH3. RhopH3 Δ 4-6 may retain sufficient activity in 50% of the parasites to
451 allow invasion to take place. Alternatively, these parasites could use a
452 RhopH3-independent pathway. Invasion by *P. falciparum* relies on several
453 redundant pathways and there is precedent for a partial reduction of
454 invasion by mutant parasites (46). It will be of interest to determine
455 whether invasion pathways that are currently thought to be redundant
456 become essential in the absence of wild type RhopH3. A third possibility is
457 that RhopH3 is involved in a post-invasion process. However, the invasion
458 assay used here would detect all intracellular parasites that have completed
459 invasion. We therefore favor the interpretation that the observed decrease
460 in the number of newly invaded *rhopH3-loxP* parasites indicates that the
461 invasion process is not completed in the mutants.

462 The other phenotype displayed by the RhopH3 Δ 4-6 mutants, the block
463 in development during the early trophozoite stage, is likely the result of a
464 defect in nutrient intake owing to improper trafficking ablating the function
465 of RhopH1/Clag. The loss of sorbitol sensitivity of erythrocytes infected with
466 the RhopH3 Δ 4-6 mutants and their impermeability to 5-ALA indicate that
467 RhopH1/Clag3.1 (the RhopH1/Clag3 isotype expressed in these 3D7-derived

468 parasites) and RhopH1/Clag3.2 are not functioning at the erythrocyte
469 surface. RhopH1/Clag3 proteins are transported to the erythrocyte surface
470 in a PEXEL-independent manner (34) and are exposed on the surface of the
471 erythrocyte (19), but the mechanism by which these proteins are
472 transported from the rhoptry, beyond the PVM and to the erythrocyte
473 plasma membrane is unknown. RhopH3 and RhopH2 are have been detected
474 in the PVM immediately after invasion, (17)(47), as well as in the
475 erythrocyte at later developmental stages of the intraerythrocytic parasite
476 (34,48). It is likely that mislocalization of RhopH3 Δ 4-6 in merozoites
477 prevents the proper, or properly timed, release of the complex during
478 invasion and prevents RhopH1/Clag from being delivered to its correct
479 location. As the RhopH1/Clag3.1 and RhopH1/Clag 3.2 in the trophozoite
480 stage parasite derives entirely from protein that is introduced during
481 invasion (15), mislocalization at the merozoite stage likely cannot be
482 corrected by additional subsequent protein synthesis.

483 The complete arrest in development of the RhopH3 Δ 4-6 mutants in
484 the cycle following gene modification (cycle 2) also provides insight into the
485 potential roles of the RhopH1/Clag proteins. Little is known about these
486 proteins other than the importance of the RhopH1/Clag3.1 and RhopH1/Clag
487 3.2 proteins in the PSAC (18). However, chemical inhibition of
488 RhopH1/Clag3.2 function and PSAC activity in parasites cultured in rich
489 medium (RPMI 1640, the same medium used in this study) leads to only a
490 small decrease in parasite viability (21). Similarly, parasites that do not
491 produce RhopH1/Clag3.1 or RhopH1/Clag 3.2 have only a minimal growth
492 disadvantage compared to wildtype parasites in a competition assay (13).

493 Parasites lacking RhopH1/Clag9 have no apparent growth phenotype *in vitro*
494 (the gene is absent from the D10 and T9-96 laboratory strains that lack part
495 of chromosome 9) (49,50). In contrast, parasites lacking RhopH1/Clag2 or
496 RhopH1/Clag8 have not been reported so the essentiality of these proteins
497 is unknown. We speculate that the RhopH3 Δ 4-6 mutants very likely transport
498 none of the RhopH1/Clag proteins to the erythrocyte surface. If so, the
499 observed growth phenotype is therefore essentially that of a disruption of
500 all the *clag* genes. The striking growth phenotype of this mutant is in stark
501 contrast to the mild phenotype of RhopH1/Clag3.2 inhibition (21) or the
502 absence of both the RhopH1/Clag3 proteins (13) when the parasites are
503 grown in RPMI. This may indicate that RhopH1/Clag2 and RhopH1/Clag8 play
504 important roles in nutrient uptake as well, as previously suggested (21), and
505 that RhopH complexes containing several different RhopH1/Clag proteins
506 together mediate the uptake of the nutrients required for parasite growth in
507 the infected erythrocyte. Interestingly, most *Plasmodium* species encode
508 fewer RhopH1/Clag proteins than *P. falciparum*; some species possess only
509 two *clag* genes, comprising a *clag9* orthologue and a second orthologue more
510 closely related to the other *P. falciparum* *clag* genes (3,10). In conclusion,
511 our results raise the intriguing possibility that, in *P. falciparum*,
512 RhopH1/Clag proteins in addition to RhopH1/Clag3.1 and RhopH1/Clag3.2
513 function in nutrient import.

514 Together the results presented in this study provide new insights into
515 the role of the rhoptry in the malarial blood stages and reveal that rhoptry
516 proteins can function in multiple, distinct processes. They furthermore show
517 that the functions of rhoptry proteins extend beyond the initial invasion of

518 the erythrocyte and can affect parasite growth throughout the blood stage
519 life cycle.

520

521 **Materials and methods**

522 **Reagents and antibodies**, Oligonucleotide primers were from Sigma-Aldrich,
523 as was rapamycin (cat# R0395), which was prepared as a 10 μ M stock in
524 DMSO. 5-aminoleuvlinic acid (5-ALA) from Sigma-Aldrich (cat# A3785) was
525 prepared as a 1 mM stock in DMSO. Restriction enzymes were from New
526 England Biolabs. The antifolate drug WR99120 (Jacobus Pharmaceuticals,
527 New Jersey, USA), was stored as a 20 μ M stock in DMSO. Polyclonal
528 antiserum α -Ag44, which recognizes the C-terminal 134 amino acid residues
529 of RhopH3 (30), was a kind gift of Ross Coppel (Monash University,
530 Australia). A polyclonal antiserum against *P. falciparum* AMA1 has been
531 previously described (51), as have polyclonal antibodies against *P.*
532 *falciparum* MSP1 and the anti-MSP1 mAb 89.1 (52). Other antibodies were
533 kindly provided by Osamu Kaneko, Nagasaki University Japan (rabbit anti-
534 RhopH1/Clag3.1A), John Vakonakis, University of Oxford UK (rabbit anti-
535 MAHRP1), Ross Coppel at Monash University Australia (anti-KAHRP), Tony
536 Holder, the Francis Crick Institute UK (anti-RhopH2 mAb 61.3). Monoclonal
537 antibody 7.7 (anti-EXP2) was from The European Malaria Reagent
538 Repository, contributed by Jana McBride and the mouse anti-RAP2 mAb
539 MRA-876 was obtained from BEI resources, National Institute of Allergy and
540 Infectious Disease (NIAID), National Institutes of Health (NIH), contributed
541 by Allan Saul. Use of these antibodies in immunoblot and IFA analyses have
542 been described elsewhere (9,11,30,51,53-56).

543

544 *P. falciparum* culture, transfection and growth analysis. All *P. falciparum*
545 transgenesis work described used the 3D7-derived DiCre-expressing clone
546 1G5DiCre (27), here referred to as 1G5DC. Asexual blood stage parasites
547 were continuously cultured in RPMI 1640 medium containing Albumax
548 (Gibco) as a serum substitute and synchronised using established procedures
549 (57). For introduction of transfection plasmids, mature schizonts were
550 enriched using Percoll (GE Healthcare) and electroporated using an Amaxa
551 4D electroporator and P3 Primary cell 4D Nucleofector X Kit L (Lonza) using
552 programme FP158 as described (27).

553 Long-term parasite growth as measured by plaque-forming ability was
554 determined by diluting trophozoite-stage cultures to a density of 10
555 parasites per well in complete medium with human erythrocytes at a
556 haematocrit of 0.75% and plating 200 μ L of this suspension into flat
557 bottomed 96 well microplates, as previously described (33). Plates were
558 incubated for 10 days in gassed humidified sealed modular chambers before
559 plaque formation was assessed by microscopic examination using a Nikon
560 TMS inverted microscope (40x magnification) and documented using a
561 Perfection V750 Pro scanner (Epson).

562 Growth characteristics of mutant parasites were determined by
563 microscopy of Giemsa-stained thin films. Long-term growth was also
564 measured using flow cytometry of hydroethidine-stained trophozoite-stage
565 parasites, as described (58). Cultures adjusted to a parasitaemia of 0.1%
566 were monitored every 48 h for up to 7 intraerythrocytic cycles. All
567 experiments were carried out in triplicate, data analysed using GraphPad

568 Prism and presented as the mean \pm standard error of the mean (SE). In
569 addition, cells 92 h post-rapamycin treatment were fixed in 4%
570 formaldehyde and 0.1% glutaraldehyde and stained with 2 μ M Hoechst 33342
571 (Invitrogen) before detection of the Hoechst emission (a measure of DNA
572 replication) by the 355 nm laser of a LSR II (BD Biosciences), through a
573 440/40 nm bandpass filter. Doublet cells were excluded using a FCS-A versus
574 FCS-H display. Samples were analysed using FlowJo software.

575 Erythrocyte invasion assays were carried out using a modification of a
576 method described previously (59). Highly synchronous, mature schizonts of
577 the parasite clones under examination were enriched by centrifugation over
578 Percoll cushions then added at a parasitaemia of 1% to fresh erythrocytes .
579 After incubation for 4 h, parasites were stained with SYBR Green-I and the
580 percentage of newly ring-infected erythrocytes was determined by flow
581 cytometry using a BD FACS Calibur flow cytometer (BD Biosciences). SYBR
582 Green-I was excited by a 488 nm 20 mW blue laser and detected by a
583 530/30 filter. BD CellQuest Pro (BD Biosciences, UK) was used to collect
584 100,000 events per sample. Experiments were done in triplicate, data
585 analysed using GraphPad Prism and presented as the mean \pm SE.

586

587 **Generation of *rhoph3-loxP* parasites and conditional RhopH3 truncation.**

588 Parasites harbouring a floxed segment of the genomic *rhoph3* gene were
589 generated by Cas9-mediated replacement of *rhoph3* endogenous introns 3
590 and 6 as well as the intervening sequence. The repair plasmid, called
591 pESS_R3_E46_loxP (synthesised by GENEWIZ) comprised synthetic
592 heterologous *loxP*-containing *SERA2* and *sub2* introns(29) flanking a

593 recodonized form of *rhoph3* exons 4-6. The complete native sequences of
594 exons 3 and 7 were included on either side of this central module to act as
595 flanking regions for homology-directed repair. Protospacer Workbench(60)
596 was used to identify 20 bp protospacer sequences specifically targeting
597 *rhoph3*. To generate pSgRNA plasmids expressing suitable sgRNAs, InFusion-
598 based cloning (Clontech) was used to replace the BtgZI adaptor sequence of
599 pL6-X(28) with annealed oligos encoding a sgRNA targeting *rhoph3* exon 4
600 (RHOPH3_sgRNA_E4_F and RHOPH3_sgRNA_E4_R, generating pSgRNA1), 5
601 (RHOPH3_sgRNA_E5_F and RHOPH3_sgRNA_E5_R, generating pSgRNA2) or 6
602 (RHOPH3_sgRNA_E6_F and RHOPH3_sgRNA_E6_R, generating pSgRNA3) (see
603 Table 2 for sequences of all oligonucleotide primers used in this study).
604 Schizonts of *P. falciparum* clone 1G5DC were transfected with 20 µg Cas9-
605 expressing pUF(28), 20 µg pESS_R3_E46_loxP repair plasmid and 8 µg of
606 sgRNA-containing pSgRNA1, pSgRNA2 or pSgRNA3. Twenty-four hours post-
607 transfection, the electroporated parasites were treated with 2.5 nM
608 WR99210 for 48 h to select for transfectants harbouring pUF1 before
609 returning the cultures to medium without drug. Integrant parasites generally
610 reached parasitaemia levels suitable for cryopreservation within 2-5 weeks.

611 Detection of integration of pESS_R3_E46_loxP in the parasite
612 population was performed by diagnostic PCR using primers
613 RHOPH3_exon2_F1 plus RHOPH3_exon5_WT_R (producing a product specific
614 to the wild type *rhoph3* locus), or RHOPH3_exon2_F1 plus RHOPH3_exon4-
615 6rec_R and RHOPH3_exon4-6rec_F plus RHOPH3_3UTR_R (producing
616 products specific to the *rhoph3-loxP* modified locus). Integrant parasite
617 clones *rhoph3-loxP* 5F5 and *rhoph3-loxP* 4B11 were then isolated by limiting

618 dilution. Persistence of the integrated DiCre locus in these clones was
619 confirmed by PCR analysis using primers +27 plus -11 producing a 1900 bp
620 product specific to the integrated DiCre cassette in 1G5DC parasites, or +27
621 plus -25 producing an amplicon of 1700 bp specific to the unmodified *SERA5*
622 locus.

623 Recombination between the *loxP* sites was induced in tightly
624 synchronised ring-stages of parasite clones *rhoph3-loxP* 5F5 and *rhoph3-*
625 *loxP* 4B11 by incubation for 4 h in the presence of 100 nM rapamycin in 1%
626 (v/v) DMSO; mock treatment was with 1% (v/v) DMSO only (vehicle control).
627 DiCre-mediated excision of the floxed *rhoph3* exons 4-6 was detected by
628 PCR analysis of schizont stage genomic DNA (harvested ~40 h following mock
629 or rapamycin treatment) using primers RHOPH3_exon2_F1 and
630 RHOPH3_exon7_R. Truncation of RhopH3 was evaluated by immunoblot
631 analysis of SDS extracts of mature Percoll-enriched schizonts, probing with
632 anti-Ag44 antibodies (or anti-AMA1 as a loading control) followed by
633 horseradish-peroxidase secondary antibodies as described(61).

634

635 **Southern blot.** For Southern blot analysis, a 738 bp probe corresponding to
636 part of *rhoph3* exon 3 was produced by PCR amplification from *P.*
637 *falciparum* IG5DC genomic DNA with primers RHOPH3_exon3_SB_F and
638 RHOPH3_exon3_SB_R (Table 2). Probe radiolabelling and hybridisation to
639 *SacI*/*BsgI*/*XmnI*-digested gDNA from clones of interest was as previously
640 described (62).

641

642 **Immunoprecipitation and immunoblot analysis.** For analysis of RhopH
643 complex formation, mature Percoll-enriched schizont-stage parasites (42 h
644 post rapamycin or mock treatment) were harvested and stored at -80 °C.
645 Frozen parasite pellets were thawed into 100 µL NP-40 lysis buffer (1%
646 Nonidet P-40, 150 mM NaCl, 50 mM Tris-HCL, 5 mM EDTA, 5 mM EGTA pH
647 8.0) containing a complete protease inhibitor cocktail (Roche). Samples
648 were clarified by centrifugation at 14,000 rpm at 4 °C and the supernatant
649 passed through a 0.22 µm cellulose acetate Spin-X centrifuge tube filter
650 (Corning). 100 µL Protein G-Sepharose beads (Abcam) were added to the
651 resulting supernatant and pre-clearing carried out at 4°C overnight.
652 Following addition of mAb 61.3 (9), samples were incubated at 4°C overnight
653 before antigen-antibody complexes were precipitated using Protein G-
654 Sepharose beads overnight at 4 °C. The beads were washed five times in
655 wash buffer I (50 mM Tris-HCl pH 8.2, 5 mM EDTA, 0.5% Nonidet P-40, 1
656 mg/mL bovine serum albumin, 0.5 M NaCl) and twice in wash buffer II (50
657 mM Tris-HCl pH 8.2, 5 mM EDTA, 0.5% Nonidet P-40) before antigen-antibody
658 complexes were eluted using NuPAGE LDS Sample Buffer (Life Technologies)
659 and proteins resolved using precast NuPAGE Novex 3-8% Tris-Acetate protein
660 gels (Life Technologies). Following electrophoresis, samples were evaluated
661 by immunoblot analysis probing with anti-Ag44 or anti-RhopH1/Clag3.1A
662 antibodies followed by horseradish-peroxidase secondary antibodies as
663 described (61).
664
665 **Immunofluorescence microscopy.** Immunofluorescence microscopy was
666 performed on formaldehyde-fixed thin blood smears, permeabilised with

667 0.1% (v/v) Triton X-100. Monoclonal anti-RAP2 (MRA-876), directly labeled
668 with Alexa Fluor 594 using the Alexa Fluor 594 Antibody Labelling Kit (Life
669 Technologies), was used at a dilution of 1:300. Samples were probed with
670 primary antibodies used at the following dilutions: anti-Ag44 (1:2000), mAb
671 61.3 (1:100), anti-CL3.1A (1:100), anti-MAHRPI (1:2000), anti-KAHRP
672 (1:250), rabbit anti-MSP1 (1:1000), mAb 89.1 (1:1000), and mAb 7.7 (1:100).
673 Bound primary antibodies were detected using Alexa Fluor 488-, 566- or 594-
674 conjugated anti-rabbit or anti-mouse secondary antibodies (Life
675 Technologies), diluted 1:8000. Slides were mounted in ProLong Gold
676 Antifade Mountant with DAPI (Life Technologies) and trophozoite images
677 captured using a Nikon Eclipse Ni-E widefield microscope with a
678 100x/1.45NA objective and a Hamamatsu C11440 digital camera. Schizont
679 stage images were captured with a Zeiss LSM 880 using a 63x/1.4 NA
680 objective equipped with an Airyscan detector to improve the optical
681 resolution of the scanned images. The DAPI, Alexa Fluor 488 and Alexa Fluor
682 594 channels were imaged sequentially over the axial dimension and
683 processed using the integrated Zeiss software to enhance the optical
684 resolution isometrically ~1.8 fold. All images were processed using either
685 the Zen 2012 or FIJI software packages. For display purposes, linear
686 adjustments were made to the intensity scale of each channel to equalize
687 the intensity output to enhance areas of co-localization. Relative intensities
688 between samples are not comparable.

689

690 Transmission electron microscopy. Parasite cultures 92 h following
691 rapamycin (or mock) treatment were fixed at 37°C in 8% formaldehyde in

692 0.2 M phosphate buffer pH 7.4 (PB) for 15 min by adding 1 volume of
693 fixative solution to 1 volume of culture. The cells were pelleted, then
694 further incubated in 2.5% glutaraldehyde, 4% formaldehyde in 0.1 M PB at
695 room temperature for a further 30 min. Cells were washed in 0.1 M PB
696 before being embedded in 4% (w/v) low-melting point agarose in distilled
697 water. The agarose-embedded samples were cut into 1 mm³ blocks, post-
698 fixed in 1% (w/v) OsO₄ and 1.5% (w/v) potassium ferrocyanide for 60 min at
699 4°C then incubated sequentially in 1% (w/v) tannic acid in 0.05 M PB for 45
700 min and 1% (w/v) sodium sulphate in 0.05 M PB for 5 min. The samples were
701 washed in water and dehydrated through a graded series of ethanol before
702 being embedded in Epon resin (Taab 812). Blocks were trimmed and
703 ultrathin 70 nm sections cut using a diamond knife on a UC6 Ultramicrotome
704 (Leica Microsystems), picked up on 150 hexagonal mesh copper grids and
705 post stained with lead citrate before being imaged using a Tecnai G2 Spirit
706 120 kV transmission electron microscope (FEI Company) with an Orius
707 camera (Gatan Inc.).

708

709 **Analysis of erythrocyte membrane permeability.** Sorbitol sensitivity of
710 parasites was determined 72 h following rapamycin or DMSO treatment (i.e.
711 in cycle 2). Cultures at equal parasitaemia were incubated in osmotic lysis
712 buffer (280 mM sorbitol, 20 mM Na-HEPES, 0.1 mg/mL BSA, pH 7.4) for 7
713 min, then hemoglobin release determined by measuring the absorbance of
714 the cell supernatants at 405 nm, as previously described(63,64).

715 5-ALA uptake was determined by incubating cultures of synchronous
716 cycle 2 ring-stage parasites overnight in phenol red-free RPMI 1640 medium

717 (K-D Medical) supplemented with 200 μ M 5-ALA. Just prior to analysis,
718 parasite nuclei were stained by treatment with 2 μ M Hoechst. PPIX and
719 Hoechst fluorescence were captured using a Zeiss LSM 880 equipped with a
720 63x/1.4 NA objective in standard confocal detection mode. Images were
721 captured with the same acquisition setting so that measurements of
722 intensity are directly comparable. Co-occurrence of PPIX and Hoechst was
723 quantified using the MetaMorph software “Cell Scoring” application. Cells
724 were also analyzed on a SORP LSRFortessa, detecting PPIX emission with a
725 532 nm laser through a 605/40 nm bandpass filter and Hoechst emission
726 with the 406 nm laser through a 440/40 nm bandpass filter. Erythrocyte
727 doublets were excluded using a FCS-A versus FCS-H display and data
728 analyzed by BD FACSDiva software.

729

730 **Time-lapse video microscopy.** *P. falciparum* egress was imaged as
731 previously described (27,65), using 1 μ M (4-[7-[(dimethylamino)methyl]-2-(4-
732 fluorophenyl)imidazo[1,2-*a*]pyridine-3-yl]pyrimidin-2-amine (compound 2) to
733 tightly synchronise egress. Following removal of compound 2 by washing,
734 parasites were suspended in fresh pre-warmed medium and introduced into
735 a pre-warmed microscopy chamber on a temperature controlled microscope
736 stage at 37°C. Beginning 6 min after washing off the compound 2, DIC
737 images were collected at 5 s intervals for 30 min using a Nikon Eclipse Ni
738 Microscope fitted with a Hamamatsu C11440 digital camera and converted
739 to QuickTime movies using Nikon NIS-Elements software.

740

741 References

742

- 743 1. WHO. (2014) World Malaria Report 2014. World Health Organization
- 744 2. Carruthers, V. B., and Sibley, L. D. (1997) Sequential protein
- 745 secretion from three distinct organelles of *Toxoplasma gondii*
- 746 accompanies invasion of human fibroblasts. *Eur. J. Cell Biol.* 73, 114-
- 747 123
- 748 3. Counihan, N. A., Kalanon, M., Coppel, R. L., and de Koning-Ward, T.
- 749 F. (2013) *Plasmodium* rhoptry proteins: why order is important.
- 750 *Trends Parasitol.* 29, 228-236
- 751 4. Zuccala, E. S., Gout, A. M., Dekiwadia, C., Marapana, D. S.,
- 752 Angrisano, F., Turnbull, L., Riglar, D. T., Rogers, K. L., Witchurch,
- 753 C. B., Ralph, S. A., Speed, T. P., and Baum, J. (2012)
- 754 Subcompartmentalisation of proteins in the rhoptries correlates with
- 755 ordered events of erythrocyte invasion by the blood stage malaria
- 756 parasite. *PLoS One* 7, e46160
- 757 5. Proellocks, N. I., Coppel, R. L., and Waller, K. L. (2010) Dissecting
- 758 the apicomplexan rhoptry neck proteins. *Trends Parasitol.* 26, 297-
- 759 304
- 760 6. Richard, D., Kats, L. M., Langer, C., Black, C. G., Mitri, K., Boddey,
- 761 J. A., Cowman, A. F., and Coppel, R. L. (2009) Identification of
- 762 rhoptry trafficking determinants and evidence for a novel sorting
- 763 mechanism in the malaria parasite *Plasmodium falciparum*. *PLoS*
- 764 *Pathogens* 5, e1000328
- 765 7. Kats, L. M., Black, C. G., Proellocks, N. I., and Coppel, R. L. (2006)
- 766 *Plasmodium* rhoptries: how things went pear-shaped. *Trends*
- 767 *Parasitol.* 22, 269-276
- 768 8. Cooper, J. A., Ingram, L. T., Bushell, G. R., Fardoulis, C. A., Stenzel,
- 769 D., Schofield, L., and Saul, A. J. (1988) The 140/130/105 kilodalton
- 770 protein complex in the rhoptries of *Plasmodium falciparum* consists of
- 771 discrete polypeptides. *Mol. Biochem Parasitol.* 29, 251-260
- 772 9. Holder, A. A., Freeman, R. R., Uni, S., and Aikawa, M. (1985)
- 773 Isolation of a *Plasmodium falciparum* rhoptry protein. *Mol. Biochem.*
- 774 *Parasitol.* 14, 293-303
- 775 10. Kaneko, O., Tsuboi, T., Ling, I. T., Howell, S., Shirano, M.,
- 776 Tachibana, M., Cao, Y. M., Holder, A. A., and Torii, M. (2001) The
- 777 high molecular mass rhoptry protein, RhopH1, is encoded by members
- 778 of the clag multigene family in *Plasmodium falciparum* and
- 779 *Plasmodium yoelii*. *Mol. Biochem. Parasitol.* 118, 223-231
- 780 11. Kaneko, O., Yim Lim, B. Y., Iriko, H., Ling, I. T., Otsuki, H., Grainger,
- 781 M., Tsuboi, T., Adams, J. H., Mattei, D., Holder, A. A., and Torii, M.
- 782 (2005) Apical expression of three RhopH1/Clag proteins as
- 783 components of the *Plasmodium falciparum* RhopH complex. *Mol.*
- 784 *Biochem. Parasitol.* 143, 20-28
- 785 12. Chung, W. Y., Gardiner, D. L., Anderson, K. A., Hyland, C. A., Kemp,
- 786 D. J., and Trenholme, K. R. (2007) The CLAG/RhopH1 locus on
- 787 chromosome 3 of *Plasmodium falciparum*: two genes or two alleles of
- 788 the same gene? *Mol. Biochem. Parasitol.* 151, 229-232
- 789 13. Comeaux, C. A., Coleman, B. I., Bei, A. K., Whitehurst, N., and
- 790 Duraisingh, M. T. (2011) Functional analysis of epigenetic regulation

- 791 of tandem RhopH1/clag genes reveals a role in *Plasmodium*
792 *falciparum* growth. *Mol. Microbiol.* 80, 378-390
- 793 14. Cortes, A., Carret, C., Kaneko, O., Yim Lim, B. Y., Ivens, A., and
794 Holder, A. A. (2007) Epigenetic silencing of *Plasmodium falciparum*
795 genes linked to erythrocyte invasion. *PLoS Pathogens* 3, e107
- 796 15. Ling, I. T., Kaneko, O., Narum, D. L., Tsuboi, T., Howell, S., Taylor,
797 H. M., Scott-Finnigan, T. J., Torii, M., and Holder, A. A. (2003)
798 Characterisation of the *rhopH2* gene of *Plasmodium falciparum* and
799 *Plasmodium yoelii*. *Mol. Biochem. Parasitol.* 127, 47-57
- 800 16. Ling, I. T., Florens, L., Dluzewski, A. R., Kaneko, O., Grainger, M.,
801 Yim Lim, B. Y., Tsuboi, T., Hopkins, J. M., Johnson, J. R., Torii, M.,
802 Bannister, L. H., Yates, J. R., 3rd, Holder, A. A., and Mattei, D.
803 (2004) The *Plasmodium falciparum clag9* gene encodes a rhoptry
804 protein that is transferred to the host erythrocyte upon invasion. *Mol.*
805 *Microbiol.* 52, 107-118
- 806 17. Sam-Yellowe, T. Y., Shio, H., and Perkins, M. E. (1988) Secretion of
807 *Plasmodium falciparum* rhoptry protein into the plasma membrane of
808 host erythrocytes. *J. Cell Biol.* 106, 1507-1513
- 809 18. Nguitrageol, W., Bokhari, A. A., Pillai, A. D., Rayavara, K., Sharma,
810 P., Turpin, B., Aravind, L., and Desai, S. A. (2011) Malaria parasite
811 *clag3* genes determine channel-mediated nutrient uptake by infected
812 red blood cells. *Cell* 145, 665-677
- 813 19. Nguitrageol, W., Rayavara, K., and Desai, S. A. (2014) Proteolysis at a
814 specific extracellular residue implicates integral membrane CLAG3 in
815 malaria parasite nutrient channels. *PloS One* 9, e93759
- 816 20. Sharma, P., Rayavara, K., Ito, D., Basore, K., and Desai, S. A. (2015)
817 A CLAG3 mutation in an amphipathic transmembrane domain alters
818 malaria parasite nutrient channels and confers leupeptin resistance.
819 *Infect. Immun.* 83, 2566-2574
- 820 21. Pillai, A. D., Nguitrageol, W., Lyko, B., Dolinta, K., Butler, M. M.,
821 Nguyen, S. T., Peet, N. P., Bowlin, T. L., and Desai, S. A. (2012)
822 Solute restriction reveals an essential role for *clag3*-associated
823 channels in malaria parasite nutrient acquisition. *Mol. Pharmacol.*
824 82, 1104-1114
- 825 22. Trenholme, K. R., Gardiner, D. L., Holt, D. C., Thomas, E. A.,
826 Cowman, A. F., and Kemp, D. J. (2000) *clag9*: A cytoadherence gene
827 in *Plasmodium falciparum* essential for binding of parasitized
828 erythrocytes to CD36. *Proc. Natl Acad. Sci. USA* 97, 4029-4033
- 829 23. Nacer, A., Roux, E., Pomel, S., Scheidig-Benatar, C., Sakamoto, H.,
830 Lafont, F., Scherf, A., and Mattei, D. (2011) Clag9 is not essential for
831 PfEMP1 surface expression in non-cytoadherent *Plasmodium*
832 *falciparum* parasites with a chromosome 9 deletion. *PloS One* 6,
833 e29039
- 834 24. Nacer, A., Claes, A., Roberts, A., Scheidig-Benatar, C., Sakamoto, H.,
835 Ghorbal, M., Lopez-Rubio, J. J., and Mattei, D. (2015) Discovery of a
836 novel and conserved *Plasmodium falciparum* exported protein that is
837 important for adhesion of PfEMP1 at the surface of infected
838 erythrocytes. *Cell. Microbiol.* 17, 1205-1216
- 839 25. Cowman, A. F., Baldi, D. L., Healer, J., Mills, K. E., O'Donnell, R. A.,
840 Reed, M. B., Triglia, T., Wickham, M. E., and Crabb, B. S. (2000)

- 841 Functional analysis of proteins involved in *Plasmodium falciparum*
842 merozoite invasion of red blood cells. *FEBS Lett.* 476, 84-88
- 843 26. Doury, J. C., Bonnefoy, S., Roger, N., Dubremetz, J. F., and
844 Mercereau-Puijalon, O. (1994) Analysis of the high molecular weight
845 rhoptry complex of *Plasmodium falciparum* using monoclonal
846 antibodies. *Parasitol.* 108 (Pt 3), 269-280
- 847 27. Collins, C. R., Das, S., Wong, E. H., Andenmatten, N., Stallmach, R.,
848 Hackett, F., Herman, J. P., Muller, S., Meissner, M., and Blackman,
849 M. J. (2013) Robust inducible Cre recombinase activity in the human
850 malaria parasite *Plasmodium falciparum* enables efficient gene
851 deletion within a single asexual erythrocytic growth cycle. *Mol.*
852 *Microbiol.* 88, 687-701
- 853 28. Ghorbal, M., Gorman, M., Macpherson, C. R., Martins, R. M., Scherf,
854 A., and Lopez-Rubio, J. J. (2014) Genome editing in the human
855 malaria parasite *Plasmodium falciparum* using the CRISPR-Cas9
856 system. *Nat. Biotechnol.* 32, 819-821
- 857 29. Jones, M. L., Das, S., Belda, H., Collins, C. R., Blackman, M. J., and
858 Treeck, M. (2016) A versatile strategy for rapid conditional genome
859 engineering using *loxP* sites in a small synthetic intron in *Plasmodium*
860 *falciparum*. *Sci. Rep.* 6, 21800
- 861 30. Coppel, R. L., Bianco, A. E., Culvenor, J. G., Crewther, P. E., Brown,
862 G. V., Anders, R. F., and Kemp, D. J. (1987) A cDNA clone expressing
863 a rhoptry protein of *Plasmodium falciparum*. *Mol. Biochem.*
864 *Parasitol.* 25, 73-81
- 865 31. Bushell, G. R., Ingram, L. T., Fardoulis, C. A., and Cooper, J. A.
866 (1988) An antigenic complex in the rhoptries of *Plasmodium*
867 *falciparum*. *Mol. Biochem. Parasitol.* 28, 105-112
- 868 32. Crewther, P. E., Culvenor, J. G., Silva, A., Cooper, J. A., and Anders,
869 R. F. (1990) *Plasmodium falciparum*: two antigens of similar size are
870 located in different compartments of the rhoptry. *Exp. Parasitol.* 70,
871 193-206
- 872 33. Thomas, J. A., Collins, C. R., Das, S., Hackett, F., Graindorge, A.,
873 Bell, D., Deu, E., and Blackman, M. J. (2016) Development and
874 application of a simple plaque assay for the human malaria parasite
875 *Plasmodium falciparum*. *PLoS One* 11, e0157873
- 876 34. Beck, J. R., Muralidharan, V., Oksman, A., and Goldberg, D. E. (2014)
877 PTEX component HSP101 mediates export of diverse malaria effectors
878 into host erythrocytes. *Nature* 511, 592-595
- 879 35. Elsworth, B., Matthews, K., Nie, C. Q., Kalanon, M., Charnaud, S. C.,
880 Sanders, P. R., Chisholm, S. A., Counihan, N. A., Shaw, P. J., Pino,
881 P., Chan, J. A., Azevedo, M. F., Rogerson, S. J., Beeson, J. G.,
882 Crabb, B. S., Gilson, P. R., and de Koning-Ward, T. F. (2014) PTEX is
883 an essential nexus for protein export in malaria parasites. *Nature*
884 511, 587-591
- 885 36. Crabb, B. S., Cooke, B. M., Reeder, J. C., Waller, R. F., Caruana, S.
886 R., Davern, K. M., Wickham, M. E., Brown, G. V., Coppel, R. L., and
887 Cowman, A. F. (1997) Targeted gene disruption shows that knobs
888 enable malaria-infected red cells to cytoadhere under physiological
889 shear stress. *Cell* 89, 287-296

- 890 37. Spycher, C., Rug, M., Pachlatko, E., Hanssen, E., Ferguson, D.,
891 Cowman, A. F., Tilley, L., and Beck, H. P. (2008) The Maurer's cleft
892 protein MAHRP1 is essential for trafficking of PfEMP1 to the surface of
893 *Plasmodium falciparum*-infected erythrocytes. *Mol. Microbiol.* **68**,
894 1300-1314
- 895 38. Babbitt, S. E., Altenhofen, L., Cobbold, S. A., Istvan, E. S., Fennell,
896 C., Doerig, C., Llinas, M., and Goldberg, D. E. (2012) *Plasmodium*
897 *falciparum* responds to amino acid starvation by entering into a
898 hibernatory state. *Proc. Natl Acad. Sci. USA* **109**, E3278-3287
- 899 39. Martin, R. E., and Kirk, K. (2007) Transport of the essential nutrient
900 isoleucine in human erythrocytes infected with the malaria parasite
901 *Plasmodium falciparum*. *Blood* **109**, 2217-2224
- 902 40. Pillai, A. D., Pain, M., Solomon, T., Bokhari, A. A., and Desai, S. A.
903 (2010) A cell-based high-throughput screen validates the plasmodial
904 surface anion channel as an antimalarial target. *Mol. Pharmacol.* **77**,
905 724-733
- 906 41. Sigala, P. A., Crowley, J. R., Henderson, J. P., and Goldberg, D. E.
907 (2015) Deconvoluting heme biosynthesis to target blood-stage malaria
908 parasites. *eLife* **4**
- 909 42. Staines, H. M., Dee, B. C., O'Brien, M., Lang, H. J., Englert, H.,
910 Horner, H. A., Ellory, J. C., and Kirk, K. (2004) Furosemide analogues
911 as potent inhibitors of the new permeability pathways of *Plasmodium*
912 *falciparum*-infected human erythrocytes. *Mol. Biochem.*
913 *Parasitol.* **133**, 315-318
- 914 43. Srinivasan, P., Beatty, W. L., Diouf, A., Herrera, R., Ambroggio, X.,
915 Moch, J. K., Tyler, J. S., Narum, D. L., Pierce, S. K., Boothroyd, J.
916 C., Haynes, J. D., and Miller, L. H. (2011) Binding of *Plasmodium*
917 *merozoite* proteins RON2 and AMA1 triggers commitment to invasion.
918 *Proc. Natl Acad. Sci. USA* **108**, 13275-13280
- 919 44. Sam-Yellowe, T. Y., and Perkins, M. E. (1990) Binding of *Plasmodium*
920 *falciparum* rhoptry proteins to mouse erythrocytes and their possible
921 role in invasion. *Mol. Biochem. Parasitol.* **39**, 91-100
- 922 45. Sam-Yellowe, T. Y., and Perkins, M. E. (1991) Interaction of the
923 140/130/110 kDa rhoptry protein complex of *Plasmodium falciparum*
924 with the erythrocyte membrane and liposomes. *Exp. Parasitol.* **73**,
925 161-171
- 926 46. Tham, W. H., Healer, J., and Cowman, A. F. (2012) Erythrocyte and
927 reticulocyte binding-like proteins of *Plasmodium falciparum*. *Trends*
928 *Parasitol.* **28**, 23-30
- 929 47. Hiller, N. L., Akompong, T., Morrow, J. S., Holder, A. A., and Haldar,
930 K. (2003) Identification of a stomatin orthologue in vacuoles induced
931 in human erythrocytes by malaria parasites. A role for microbial raft
932 proteins in apicomplexan vacuole biogenesis. *J. Biol. Chem.* **278**,
933 48413-48421
- 934 48. Vincensini, L., Fall, G., Berry, L., Blisnick, T., and Braun Breton, C.
935 (2008) The RhopH complex is transferred to the host cell cytoplasm
936 following red blood cell invasion by *Plasmodium falciparum*. *Mol.*
937 *Biochemical Parasitol.* **160**, 81-89
- 938 49. Chaiyaroj, S. C., Coppel, R. L., Magowan, C., and Brown, G. V. (1994)
939 A *Plasmodium falciparum* isolate with a chromosome 9 deletion

- 940 expresses a trypsin-resistant cytoadherence molecule. *Mol. Biochem.*
941 *Parasitol* 67, 21-30
- 942 50. Day, K. P., Karamalis, F., Thompson, J., Barnes, D. A., Peterson, C.,
943 Brown, H., Brown, G. V., and Kemp, D. J. (1993) Genes necessary for
944 expression of a virulence determinant and for transmission of
945 *Plasmodium falciparum* are located on a 0.3-megabase region of
946 chromosome 9. *Proc. Natl Acad. Sci. USA* 90, 8292-8296
- 947 51. Collins, C. R., Withers-Martinez, C., Hackett, F., and Blackman, M. J.
948 (2009) An inhibitory antibody blocks interactions between
949 components of the malarial invasion machinery. *PLoS Pathogens* 5,
950 e1000273
- 951 52. Holder, A. A., Lockyer, M. J., Odink, K. G., Sandhu, J. S., Riveros-
952 Moreno, V., Nicholls, S. C., Hillman, Y., Davey, L. S., Tizard, M. L.,
953 Schwarz, R. T., and et al. (1985) Primary structure of the precursor
954 to the three major surface antigens of *Plasmodium falciparum*
955 merozoites. *Nature* 317, 270-273
- 956 53. Hall, R., McBride, J., Morgan, G., Tait, A., Zolg, J. W., Walliker, D.,
957 and Scaife, J. (1983) Antigens of the erythrocytes stages of the
958 human malaria parasite *Plasmodium falciparum* detected by
959 monoclonal antibodies. *Mol. Biochem. Parasitol.* 7, 247-265
- 960 54. Oberli, A., Slater, L. M., Cutts, E., Brand, F., Mundwiler-Pachlatko,
961 E., Rusch, S., Masik, M. F., Erat, M. C., Beck, H. P., and Vakonakis, I.
962 (2014) A *Plasmodium falciparum* PHIST protein binds the virulence
963 factor PfEMP1 and comigrates to knobs on the host cell surface.
964 *FASEB J.* 28, 4420-4433
- 965 55. Pei, X., An, X., Guo, X., Tarnawski, M., Coppel, R., and Mohandas, N.
966 (2005) Structural and functional studies of interaction between
967 *Plasmodium falciparum* knob-associated histidine-rich protein
968 (KAHRP) and erythrocyte spectrin. *J. Biol. Chem.* 280, 31166-31171
- 969 56. Saul, A., Cooper, J., Hauquitz, D., Irving, D., Cheng, Q., Stowers, A.,
970 and Limpitboon, T. (1992) The 42-kilodalton rhoptry-associated
971 protein of *Plasmodium falciparum*. *Mol. Biochem. Parasitol.* 50, 139-
972 149
- 973 57. Blackman, M. J. (1994) Purification of *Plasmodium falciparum*
974 merozoites for analysis of the processing of merozoite surface
975 protein-1. *Methods Cell Biol.* 45, 213-220
- 976 58. Stallmach, R., Kavishwar, M., Withers-Martinez, C., Hackett, F.,
977 Collins, C. R., Howell, S. A., Yeoh, S., Knuepfer, E., Atid, A. J.,
978 Holder, A. A., and Blackman, M. J. (2015) *Plasmodium falciparum*
979 SERA5 plays a non-enzymatic role in the malarial asexual blood-stage
980 lifecycle. *Mol. Microbiol.* 96, 368-387
- 981 59. Moss, D. K., Remarque, E. J., Faber, B. W., Cavanagh, D. R., Arnot,
982 D. E., Thomas, A. W., and Holder, A. A. (2012) *Plasmodium*
983 *falciparum* 19-kilodalton merozoite surface protein 1 (MSP1)-specific
984 antibodies that interfere with parasite growth in vitro can inhibit
985 MSP1 processing, merozoite invasion, and intracellular parasite
986 development. *Infect. Imm.* 80, 1280-1287
- 987 60. MacPherson, C. R., and Scherf, A. (2015) Flexible guide-RNA design
988 for CRISPR applications using Protospacer Workbench. *Nat.*
989 *Biotechnol.* 33, 805-806

990 61. Jean, L., Hackett, F., Martin, S. R., and Blackman, M. J. (2003)
991 Functional characterization of the propeptide of *Plasmodium*
992 *falciparum* subtilisin-like protease-1. *J. Biol. Chem.* 278, 28572-
993 28579

994 62. Ruecker, A., Shea, M., Hackett, F., Suarez, C., Hirst, E. M.,
995 Milutinovic, K., Withers-Martinez, C., and Blackman, M. J. (2012)
996 Proteolytic activation of the essential parasitophorous vacuole
997 cysteine protease SERA6 accompanies malaria parasite egress from its
998 host erythrocyte. *J. Biol. Chem.* 287, 37949-37963

999 63. Ginsburg, H., Kutner, S., Krugliak, M., and Cabantchik, Z. I. (1985)
1000 Characterization of permeation pathways appearing in the host
1001 membrane of *Plasmodium falciparum* infected red blood cells. *Mol.*
1002 *Biochem. Parasitol.* 14, 313-322

1003 64. Kirk, K., Horner, H. A., Elford, B. C., Ellory, J. C., and Newbold, C. I.
1004 (1994) Transport of diverse substrates into malaria-infected
1005 erythrocytes via a pathway showing functional characteristics of a
1006 chloride channel. *J. Biol. Chem.* 269, 3339-3347

1007 65. Das, S., Hertrich, N., Perrin, A. J., Withers-Martinez, C., Collins, C.
1008 R., Jones, M. L., Watermeyer, J. M., Fobes, E. T., Martin, S. R.,
1009 Saibil, H. R., Wright, G. J., Treeck, M., Epp, C., and Blackman, M. J.
1010 (2015) Processing of *Plasmodium falciparum* merozoite surface
1011 protein MSP1 activates a spectrin-binding function enabling parasite
1012 egress from RBCs. *Cell Host Microbe* 18, 433-444
1013
1014
1015

1016

1017

1018 **Acknowledgements**

1019 This work was supported by the Francis Crick Institute, which receives its
1020 core funding from Cancer Research UK (FC001043), the UK Medical Research
1021 Council (FC001043), and the Wellcome Trust (FC001043). ESS was supported
1022 by a Wellcome Trust/NIH PhD studentship (013459/Z/14/Z) and CvO was
1023 supported by a Wellcome Trust Career Re-Entry Fellowship
1024 (095836/Z/11/Z). This research was also supported in part by the Intramural
1025 Research Program of the National Institute of Allergy and Infectious
1026 Diseases, National Institutes of Health. The authors are indebted to Anne
1027 Weston of the Electron Microscopy Science Technology Platform at the
1028 Francis Crick Institute, Fiona Hackett (Francis Crick Institute) for assistance
1029 with parasite culture, J. J. Lopez-Rubio (University of Montpellier) for
1030 sharing the pL6 and pUF1 plasmids and David Stephany and Kevin Holmes
1031 (Flow Cytometry Core, Research and Technologies Branch, National Institute
1032 of Allergy and Infectious Disease) for assistance with cell analysis. The
1033 following generously provided antibodies: R. Coppel, O. Kaneko, A. Holder,
1034 J. Vakonakis, BEI resources via contribution from A. Saul and The European
1035 Malaria Reagent Repository via contribution from J. McBride.

1036

1037

1038

1039 **Author contributions**

1040 E.S.S., M.J.B. and C.v.O. conceived and designed the experiments. E.S.S.
1041 performed the experiments and analysed the data. E.K. designed the
1042 Southern blotting strategy and J.A.B. assisted with image acquisition.
1043 L.H.M., M.J.B. and C.v.O. supervised the project. E.S.S., M.J.B. and C.v.O.
1044 wrote the manuscript.

1045

1046 **Competing financial interest**

1047 The authors declare no competing financial interest.

1048

1049 **Corresponding authors**

1050 Correspondence and requests for materials should be addressed to M.J.B.

1051 (Mike.Blackman@crick.ac.uk) or C.v.O. (Christiaan.vanOoij@crick.ac.uk)

1052

1053

1054

1055
1056
1057
1058
1059
1060
1061

Table 1. Conditional truncation of RhopH3 results in decreased parasite survival as determined by plaque assay.

^a Plaque assay no.	Treatment	^b Proportion of wells containing plaques (%)	Mean number of plaques/well
1 (clone 5F5)	DMSO	98.88	7.7
	Rapamycin	10.56	0.11
2 (clone 5F5)	DMSO	100	9.1
	Rapamycin	8.89	0.09
3 (clone 4B11)	DMSO	99.44	5.24
	Rapamycin	9.44	0.1

1062
1063
1064
1065
1066
1067
1068

^a Three independent plaque assays were set up on different days.

^b A total of 180 wells were used for each treatment (+/-RAP) in each assay.

1069
 1070
 1071
 1072
 1073
 1074

Table 2. Oligonucleotide primers used in this study. Guide sequences shown in bold.

Primer name	Sequence (5'-3')
RHOPH3_sgRNA_E4_F*	taagtataatatt TTCTTCGTTTTTAAAAAAG gtttagagctagaa
RHOPH3_sgRNA_E4_R*	ttctagctctaaac CTTTTTTAAAAACGAAGAA aatattatatactta
RHOPH3_sgRNA_E5_F*	taagtataatatt CACCGATTTTAGCTTTAAAG gtttagagctagaa
RHOPH3_sgRNA_E5_R*	ttctagctctaaac CTTTAAAGCTAAAATCGGT Gaatattatatactta
RHOPH3_sgRNA_E6_F*	taagtataatatt ACATTCTTATCATTATATTT gtttagagctagaa
RHOPH3_sgRNA_E6_R*	ttctagctctaaac ACATTCTTATCATTATATTT aatattatatactta
RHOPH3_exon2_F1	AGGAAATGGCCCAGACGC
RHOPH3_exon5_WT_R	TCTTTAAAGCTAAAATCGGTGATATTATGGCTC
RHOPH3_exon4-6rec_R	CAGGAAGTTACCTTTCAGCAGGG
RHOPH3_exon4-6rec_F	CCCTGCTGAAAGGTAACCTCCTG
RHOPH3_3UTR_R	CGAATATGTAATCAGTTGTATTTTTCTCTAAAAGTTCATAG
+27	CAATATCATTTGAATCAAACAGTGGT
-11	CTTTGCCATCCAGGCTGTTC
-25	CCATTGGACTAGAACCTTCAT
RHOPH3_exon7_R	CATAAAGAACGTCTTGTTTTCTGTATCCAATACC
RHOPH3_exon3_SB_F	CAAATATGCTATATGTGTAGGTA CTCAATTTAAC
RHOPH3_exon3_SB_R	CATATAACTTTGGAGATGTAGAACCAAGG

1075

1076 **Figure legends**

1077 **Figure 1** Conditional truncation of the *rhoph3* gene. A) The *rhoph3* gene
1078 comprises seven exons (numbered grey boxes) and six introns (blue lines).
1079 Using Cas9-mediated recombination, the region spanning introns 3 through 6
1080 was replaced with two *loxP*-containing (purple open arrowhead) *P. falciparum*
1081 introns (*SERA2* (orange line) and *sub2* (green line)) flanking a
1082 recodonized and fused version of exons 4 through 6 (exon 4-6, green box).
1083 Integration of this sequence by homologous recombination was promoted by
1084 the addition sequences of exon 3 and 7 to either side of the introns. Colored
1085 arrowheads, primer binding sites. B, S and X, BsgI, SacI and XmnI restriction
1086 sites. Dotted line, probe used for Southern blotting. Rapamycin-induced
1087 site-specific recombination between the *loxP* sites removes the recodonized
1088 exon 4-6. B) PCR analysis of *rhoph3-loxP* clones 5F5 and 4B11 confirms the
1089 expected gene modification event. Genomic DNA from parental 1G5DC (WT)
1090 parasites or the clones was used as template for PCR using the indicated
1091 primers (see panel A). Numbers between the arrowheads indicate the
1092 expected size of the amplicon. C) Southern blot analysis of parental 1G5DC
1093 (WT) and the *rhoph3-loxP* parasite clones confirms the expected
1094 modification of the *rhoph3* locus. Genomic DNA was digested with BsgI, SacI
1095 and XmnI and hybridized with a radiolabeled probe that binds to part of
1096 exon 3 (dotted line in panel A). Expected fragment sizes are 3016 bp for the
1097 WT *rhoph3* locus and 3349 bp for the *rhoph3-loxP* locus. D) Efficient
1098 rapamycin-induced truncation of the *rhoph3* gene. Clones *rhoph3-loxP* 5F5
1099 and 4B11 were analyzed by PCR ~44 h after treatment with DMSO (D) or
1100 rapamycin (R) using the indicated primers (see panel A). Excision decreases

1101 the amplicon from 2760 bp to 1755 bp. E) Southern blot showing efficient
1102 rapamycin-induced truncation of the *rhopH3* gene. Genomic DNA extracted
1103 from control or rapamycin-treated *rhopH3-loxP* clones 5F5 and 4B11 was
1104 digested and probed as described in panel C. Expected fragment sizes are
1105 3349 bp for the non-excised locus and 4784 bp for the excised locus. F)
1106 Immunoblot analysis of mature schizonts of *rhopH3-loxP* clone 5F5,
1107 examined ~44 h following treatment at ring stage with DMSO (D) or
1108 rapamycin (R). The blots were probed with an antibody against RhopH3 (left
1109 panel) or the merozoite protein AMA1 (right panel) as a loading control. The
1110 expected molecular masses of WT RhopH3 and RhopH3 Δ 4-6 are 110 kDa and
1111 ~70 kDa, respectively. In panels B-F, positions of relevant molecular mass
1112 markers are indicated.

1113

1114 **Figure 2** Truncation of RhopH3 leads to mistrafficking of components of the
1115 RhopH complex and loss of complex formation. A) IFA showing colocalization
1116 of RhopH3, RhopH2 and RhopH1/Clag3.1 with the rhoptry marker RAP2 in
1117 schizonts of control (DMSO) *rhopH3-loxP* parasites but loss of colocalization
1118 following rapamycin (Rapa) treatment. Parasite nuclei were visualized by
1119 staining with 4,6-diamidino-2-phenylindole (DAPI). Scale bar, 5 μ m. B)
1120 Colocalization of the members of the RhopH complex. RhopH3, RhopH2 and
1121 RhopH1/Clag3.1 colocalize in *rhopH3-loxP* parasites treated with DMSO, but
1122 this colocalization is lost in parasites treated with rapamycin. C)
1123 Mislocalisation and reduced levels of RhopH3 in naturally released free
1124 merozoites of *rhopH3-loxP* parasites treated with rapamycin. Samples were
1125 probed with a monoclonal antibody to the merozoite surface marker MSP1

1126 as well as anti-RhopH3 antibodies. Scale bar, 2 μ m D) Immunoprecipitation
1127 reveals disruption of the RhopH complex in rapamycin-treated *rhoph3-loxP*
1128 parasites. RhopH2 was immunoprecipitated from extracts of control or
1129 rapamycin-treated *rhoph3-loxP* parasites. Subsequent immunoblotting with
1130 antibodies against RhopH3 or RhopH1/Clag3.1 revealed the absence of
1131 RhopH3 from the immunoprecipitates derived from the rapamycin-treated
1132 parasites, although RhopH2 and RhopH1/Clag3.1 still showed association.
1133 Arrowheads indicate the expected position of migration of the full-length
1134 (WT) and truncated RhopH3, and RhopH1/Clag3.1. The *rhoph3-loxP* clone
1135 5F5 was used throughout for these experiments.

1136

1137 **Figure 3** Loss of long-term viability in parasites lacking the RhopH complex.

1138 A) Representative wells seeded with identical concentrations (10 parasitised
1139 cells/well) of DMSO-treated or rapamycin-treated *rhoph3-loxP* clone 5F5
1140 parasites, showing formation of plaques only in the wells seeded with DMSO-
1141 treated parasites. Two of the plaques are indicated by white arrowheads. B)
1142 PCR analysis of the *rhoph3-loxP* locus in the small number of clones isolated
1143 from wells seeded with rapamycin-treated *rhoph3-loxP* parasites. The size
1144 of the PCR product indicates excision of the floxed sequence had not taken
1145 place in these seven clones (numbered 1-7), whereas rapamycin induced
1146 efficient excision in the parent 5F5 clone (left-hand two tracks). For PCR
1147 strategy, see Figure 1D. C) PCR analysis of the modified *SERA5* locus in
1148 parasite clone RhopH3 NE, showing loss of the DiCre cassette in this clone.
1149 D) Growth curves showing replication of parasites of the indicated clones
1150 over the course of 5 erythrocytic cycles. Data were averaged from 3

1151 biological replicate experiments and presented as the mean \pm standard error
1152 of the mean. E) Non-excised parasites quickly outgrow RhopH3 Δ 4-6
1153 parasites. The relative abundance of parasites harboring the excised or
1154 intact *rhopH3-loxP* locus in a population of rapamycin-treated *rhopH3-loxP*
1155 clone 5F5 parasites was determined by diagnostic PCR over the course of 7
1156 erythrocytic growth cycles (indicated, where cycle 1 indicates that in which
1157 treatment occurred). F) Decreased erythrocyte invasion by rapamycin-
1158 treated *rhopH3-loxP* parasites. Parasites of the indicated clones were
1159 treated with DMSO or rapamycin and allowed to invade fresh erythrocytes.
1160 Ring-stage parasitemia levels were determined 4 h later. Data were
1161 averaged from 3 biological replicate experiments. Error bars depict standard
1162 error of the mean. Statistical significance was determined by a two-tailed t-
1163 test where $p \leq 0.0001$ (indicated by asterisks) and $p > 0.05$, non-significant
1164 (ns).

1165

1166 **Figure 4** Loss of the RhopH complex results in developmental arrest. A)
1167 Developmental block in rapamycin-treated *rhopH3-loxP* parasites. Giemsa-
1168 stained images showing intracellular development of DMSO-treated and
1169 rapamycin-treated *rhopH3-loxP* clone 5F5 parasites from the end of cycle 1
1170 to the end of cycle 2. A clear developmental block was evident in the
1171 rapamycin-treated parasites in cycle 2. The number of hours following the
1172 beginning of cycle 1 is indicated, as well as its relation to the time point of
1173 rapamycin treatment (indicated in the schematic timeline). B) Flow
1174 cytometry analysis of DMSO-treated and rapamycin-treated *rhopH3-loxP*
1175 clones 5F5 and 4B11. Analysis was performed at the end of the cycle 2 (92 h

1176 after rapamycin-treatment). The intensity of Hoechst 33342 staining
1177 provides a measure of the DNA content of the parasites, reflecting parasite
1178 development.

1179

1180 **Figure 5** Loss of the RhopH complex does not ablate parasite protein export.

1181 Cycle 2 (72 h post rapamycin treatment) DMSO-treated and rapamycin-

1182 treated *rhopH3-loxP* clone 5F5 trophozoite-stage parasites were probed with

1183 antibodies against the parasitophorous vacuole membrane marker EXP2 to

1184 delineate the parasite in the infected erythrocyte, as well as antibodies

1185 specific for either the Maurer's cleft marker MAHRP1 (top panels) or the

1186 export marker KAHRP (bottom panels). Scale bar, 5 μ m. B) Transmission

1187 electron micrograph showing a comparison between cycle 2 parasites of

1188 DMSO-treated or rapamycin-treated *rhopH3-loxP* clone 5F5 parasites ~ 92 h

1189 following rapamycin treatment. The developmental block in the RhopH3 Δ 4-6

1190 parasite is clearly evident, as is the presence of knobs (arrowed) on the

1191 surface of the erythrocyte in both cases. Components of the mutant parasite

1192 labelled are the digestive vacuole (DV), haemozoin (H), nucleus (N),

1193 parasitophorous vacuole membrane (PVM), cytostomes (C) and parasite

1194 plasma membrane (PPM). The mutant parasites displayed no obvious

1195 ultrastructural differences from wild-type trophozoites at a similar

1196 developmental stage (not shown). Scale bar, 1 μ m

1197

1198 **Figure 6** Loss of the RhopH complex results in reduced sorbitol sensitivity

1199 and reduced uptake of exogenous small molecules. A) Synchronous cycle 2

1200 parasites of the indicated clone (parasitaemia ~5%) treated 72 h previously

1201 with DMSO or rapamycin in cycle 1 were suspended in osmotic lysis buffer
1202 containing 280 mM sorbitol or in PBS, and the resulting cell lysis determined
1203 by measuring the absorbance of the supernatant at 405 nm. An equal
1204 volume of parasite culture was lysed in 0.15% (w/v) saponin to give a value
1205 for 100% lysis and all other absorbance values normalized to this. Data were
1206 averaged from 3 biological replicate experiments. Statistical significance
1207 was determined by a two-tailed t-test; significance levels are indicated:
1208 $p \leq 0.001$, ***; $p \leq 0.01$, **; $p \leq 0.05$, *; and $p > 0.05$, non-significant (ns). B)
1209 Uptake of 5-ALA by erythrocytes infected with either DMSO-treated or
1210 rapamycin-treated *rhoph3-loxP* clone 5F5 parasites at cycle 2. Cultures
1211 were incubated overnight with 200 μ M 5-ALA and uptake of the compound
1212 and its subsequent conversion to PPIX in infected erythrocytes visualized
1213 by fluorescence microscopy. Infected erythrocytes were visualized by
1214 staining with Hoechst 33342. Top panels show fields of view containing
1215 multiple infected erythrocytes of the indicated strain. Scale bar, 50 μ m
1216 Bottom panels show individual infected erythrocytes. Scale bar, 5 μ m. C)
1217 Quantitation of the levels of uptake of 5-ALA by infected erythrocytes. For
1218 each condition, a total of 1300 Hoechst-positive cells were analyzed for
1219 intensity of PPIX fluorescence using MetaMorph (Molecular Devices) and a
1220 statistical significance was determined by a two-tailed t-test. Significance
1221 levels are indicated: $p \leq 0.0001$, **** and $p > 0.05$, non-significant (ns). D) FACS
1222 analysis of 5-ALA-treated parasites. Uptake of 5-ALA and its subsequent
1223 conversion to PPIX in cycle 2 parasites following treatment in cycle 1 with
1224 rapamycin or DMSO was determined by flow cytometry of Hoechst stained
1225 parasites. Gating was applied to distinguish Hoechst negative cells (red

1226 population), Hoechst positive/PPIX negative cells (green population) and
1227 Hoechst positive/PPIX-positive cells (purple population). For the 1G5DC
1228 parental and RhopH3-loxP NE parasite clones, most of the parasites were
1229 positive for both Hoechst and PPIX fluorescence regardless of their
1230 treatment with rapamycin or DMSO. In contrast, for rapamycin-treated
1231 *rhopH3-loxP* clones 5F5 and 4B11, most of the parasites were Hoechst
1232 positive/PPIX negative indicating a defect in 5-ALA uptake.

1233
1234
1235

1236 Supplemental figure legends.

1237

1238 **Figure 1 - figure supplement 1.** Multiple alignment of predicted primary
1239 sequences of *rhoph3* orthologues from *P. falciparum* (PF3D7_0905400), *P.*
1240 *chabaudi* (PCHAS_0416900) and *P. vivax* (PVX_098712). The portion of the
1241 protein encoded by exon 4-6 in the *P. falciparum* orthologue is underlined.
1242 Note that this region includes some of the most highly conserved regions of
1243 the protein. Sequence data were obtained from PlasmoDB (1) and aligned
1244 using Clustal Omega (2). ‘*’ indicates positions of identity, ‘:’ indicates
1245 conservation of residues with strongly similar chemical properties and ‘.’
1246 indicates conservation of residues of weakly similar properties.

1247

1248 **Figure 1 - figure supplement 2.** Modification (floxing) of the *rhoph3* gene
1249 does not impact on gene expression or parasite growth. A) Immunoblot
1250 analysis of untreated mature schizonts of *rhoph3-loxP* clones 5F5 and 4B11,
1251 as well as the RhopH3 NE clone and the parental 1G5DC parasites. The blots
1252 were probed with an antibody against RhopH3 (top), RhopH1/Clag3.1
1253 (middle) or the merozoite protein EBA175 (3) (bottom) as a loading control.
1254 B) Growth curves showing similar replication rates of parasites of the
1255 indicated clones (not treated with rapamycin) over the course of 4
1256 erythrocytic cycles. Data were averaged from 3 biological replicate
1257 experiments and presented as the mean \pm standard error of the mean.
1258 Linear regression analysis showed that all the slopes fall within the same
1259 95% confidence interval range.

1260

1261 **Figure 1 - figure supplement 3.** Conditional truncation of RhopH3 in both
1262 the 5F5 and 4B11 *rhopH3-loxP* clones. Immunoblot analysis of mature
1263 schizonts of the indicated clones ~44 h following treatment at ring stage
1264 with DMSO (D) or rapamycin (R). The blots were probed with an antibody
1265 against RhopH3 (top) or the mAb 89.1 against the merozoite surface protein
1266 MSP1 (bottom) as a loading control. The expected molecular masses of WT
1267 RhopH3 and RhopH3 Δ 4-6 are 110 kDa and ~70 kDa, respectively. Positions of
1268 relevant molecular mass markers are indicated.

1269

1270 **Figure 2 - figure supplement 1.** Truncation of RhopH3 leads to
1271 mistrafficking of components of the RhopH complex. IFA of mature schizonts
1272 of control (DMSO) and rapamycin-treated *rhopH3-loxP* parasites, probed
1273 with MSP1-specific antibodies (either mAb 89.1 or rabbit polyclonal anti-
1274 MSP1 antibodies; red) and antibodies to the three indicated RhopH
1275 components (green). Mis-localisation of the RhopH proteins was observed in
1276 all cases, and in the case of RhopH3 the protein often appeared to reside
1277 external to the plasma membrane of intracellular merozoites. Parasite
1278 nuclei were visualized by staining with DAPI. Note that, for clarity, the
1279 merge panels do not include the DAPI signal. Scale bar, 5 μ m.

1280

1281 **Supplementary figure references**

1282 1. Aurrecochea, C., Brestelli, J., Brunk, B. P., Dommer, J., Fischer, S., Gajria, B.,
1283 Gao, X., Gingle, A., Grant, G., Harb, O. S., Heiges, M., Innamorato, F., Iodice,
1284 J., Kissinger, J. C., Kraemer, E., Li, W., Miller, J. A., Nayak, V., Pennington, C.,
1285 Pinney, D. F., Roos, D. S., Ross, C., Stoeckert, C. J., Jr., Treatman, C., and
1286 Wang, H. (2009) PlasmoDB: a functional genomic database for malaria
1287 parasites. *Nucleic Acids Res.* **37**, D539-543

- 1288 2. Sievers, F., Wilm, A., Dineen, D., Gibson, T. J., Karplus, K., Li, W., Lopez, R.,
1289 McWilliam, H., Remmert, M., Soding, J., Thompson, J. D., and Higgins, D. G.
1290 (2011) Fast, scalable generation of high-quality protein multiple sequence
1291 alignments using Clustal Omega. *Mol. Syst. Biol.* **7**, 539
- 1292 3. O'Donnell, R. A., Hackett, F., Howell, S. A., Treeck, M., Struck, N., Krnajski, Z.,
1293 Withers-Martinez, C., Gilberger, T. W., and Blackman, M. J. (2006)
1294 Intramembrane proteolysis mediates shedding of a key adhesin during
1295 erythrocyte invasion by the malaria parasite. *J. Cell Biol.* **174**, 1023-1033
1296
- 1297

1298 **Supplementary Video 1** Parasite egress is unaffected by loss of the RhopH
1299 complex. Synchronized parasites of *rhopH3-loxP* clone 4B11 were treated
1300 with DMSO or rapamycin at ring stage, then allowed to mature to schizont
1301 stage and further synchronised by incubation for 3-5 h in the presence of 1
1302 μM (4-[7-[(dimethylamino)methyl]-2-(4-fluorophenyl)imidazo[1,2-*a*]pyridine-
1303 3-yl]pyrimidin-2-amine (compound 2), which reversibly stalls egress. Egress
1304 of the parasites was then monitored by time-lapse DIC video microscopy
1305 following removal of the compound 2, as described previously¹. DMSO-
1306 treated samples are shown on the left, rapamycin-treated are samples
1307 shown on the right.

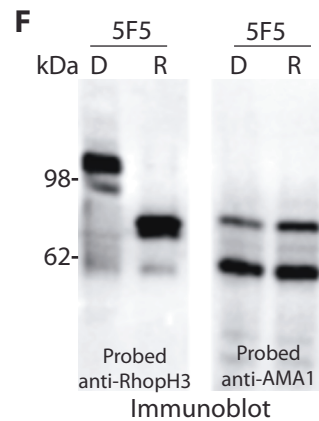
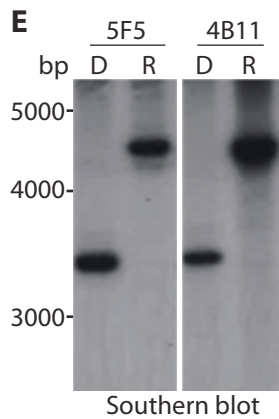
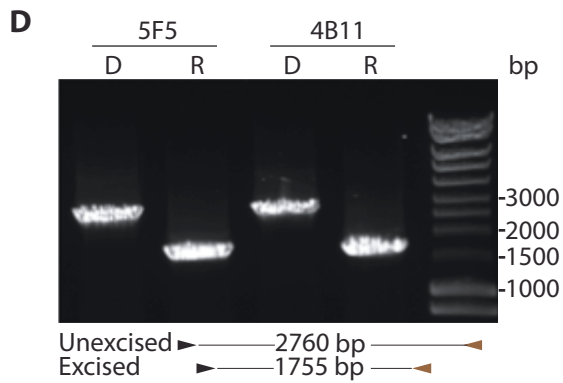
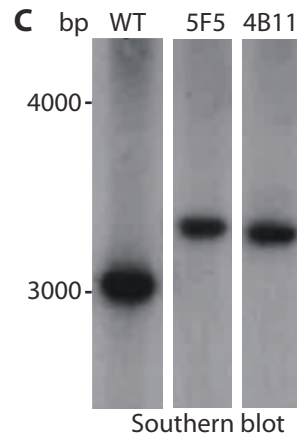
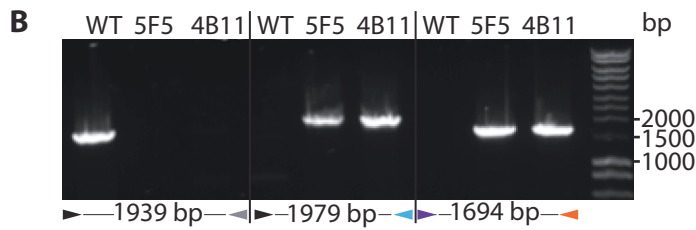
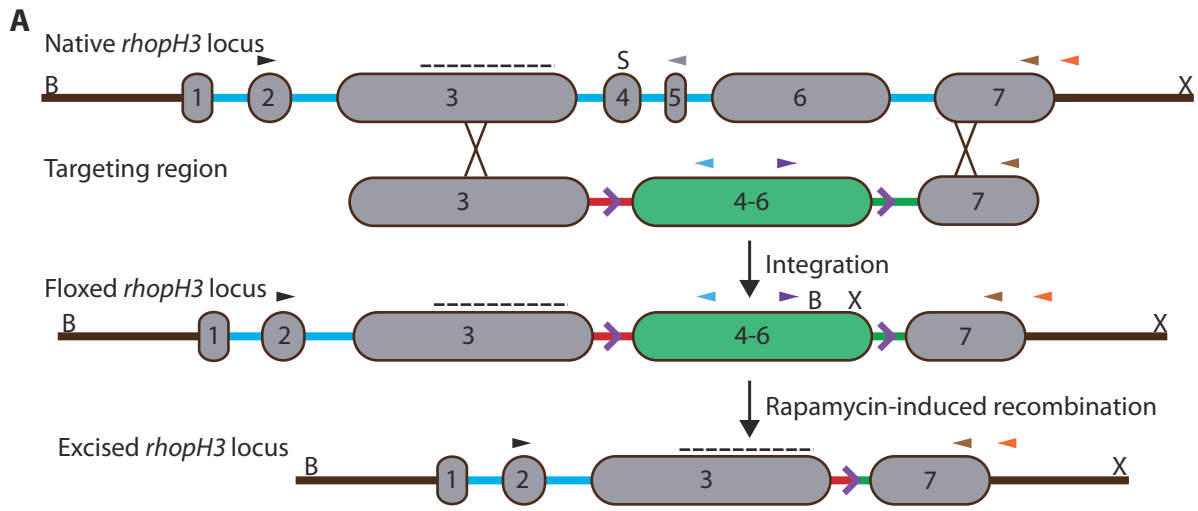
1308

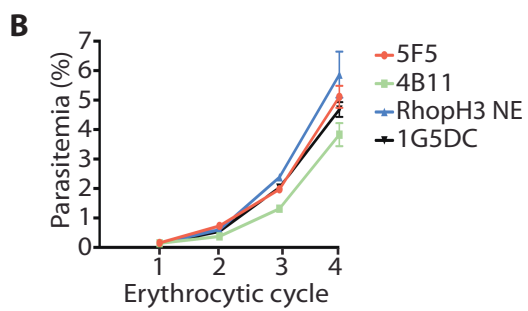
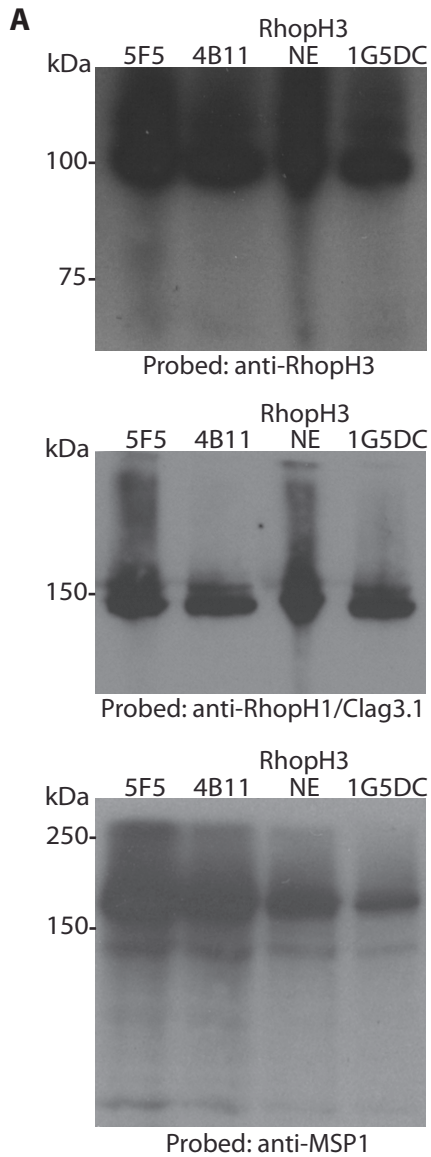
1309 **Supplementary video reference**

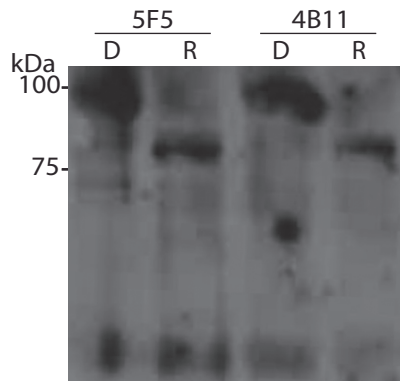
1310

- 1311 1. Das, S., Hertrich, N., Perrin, A. J., Withers-Martinez, C., Collins, C.
1312 R., Jones, M. L., Watermeyer, J. M., Fobes, E. T., Martin, S. R.,
1313 Saibil, H. R., Wright, G. J., Treeck, M., Epp, C., and Blackman, M. J.
1314 (2015) Processing of *Plasmodium falciparum* merozoite surface
1315 protein MSP1 activates a spectrin-binding function enabling parasite
1316 egress from RBCs. *Cell Host Microbe* 18, 433-444

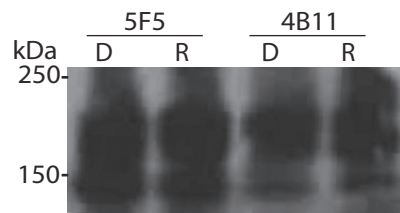
1317



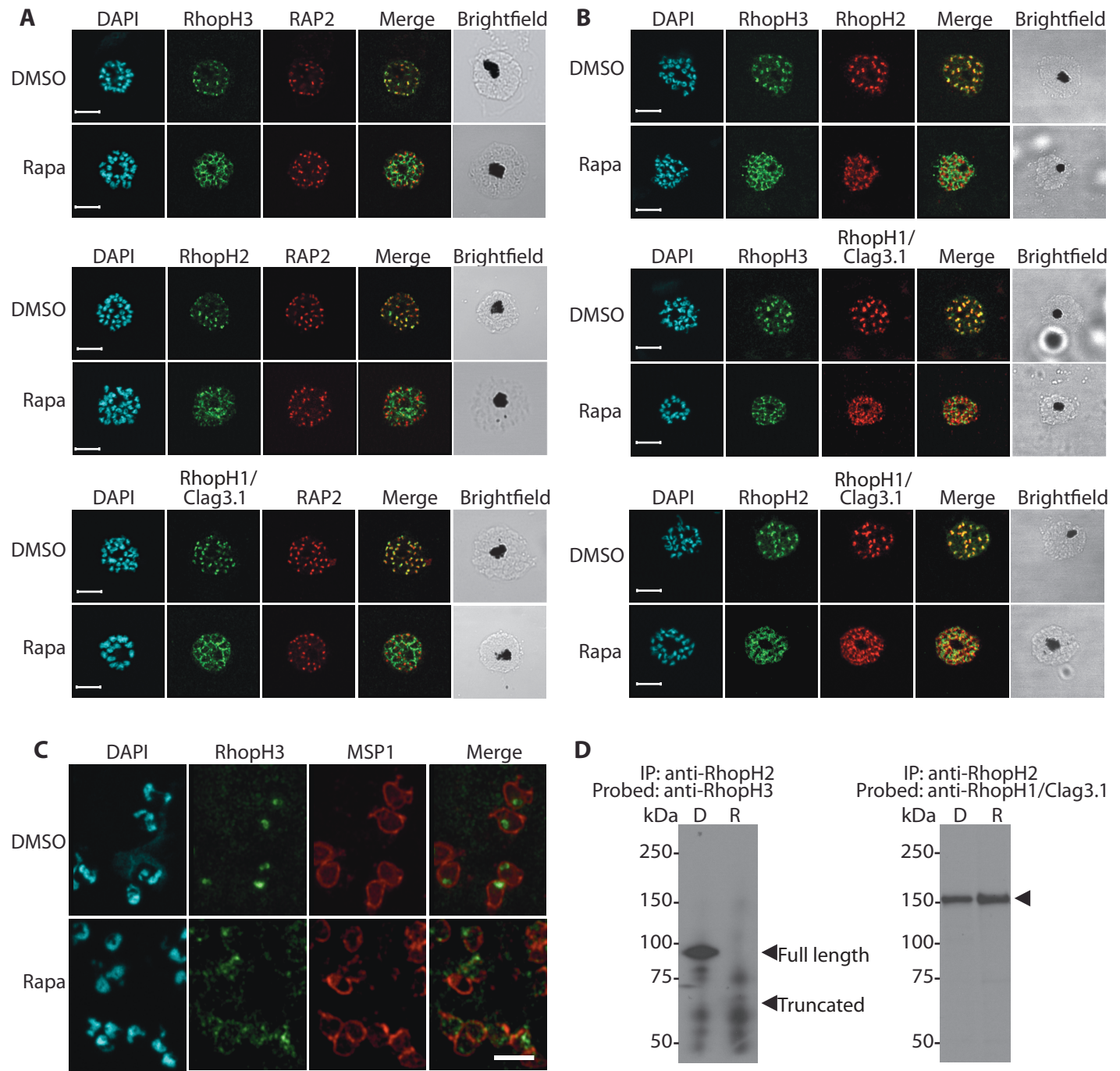


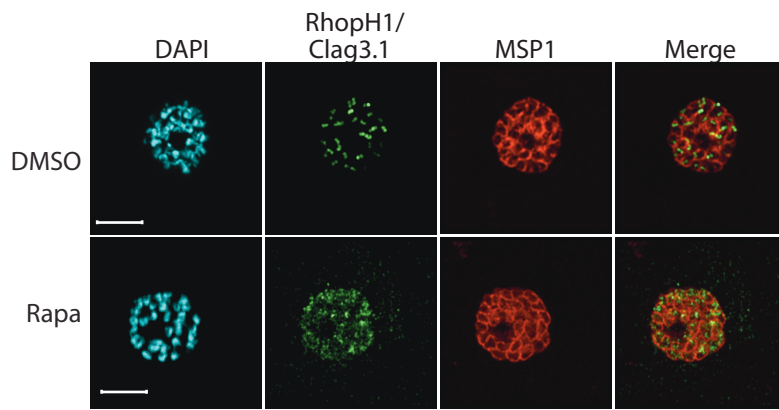
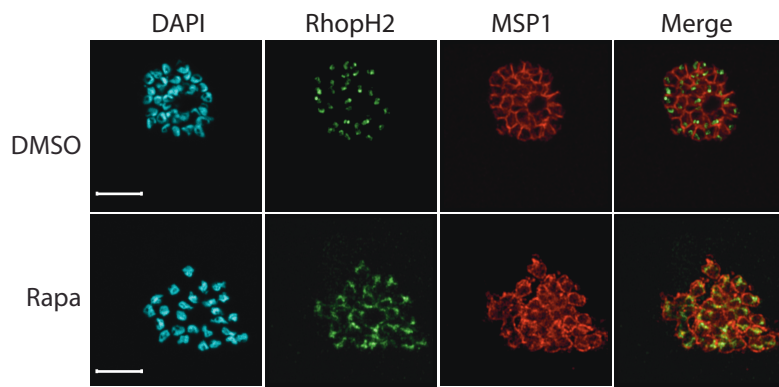
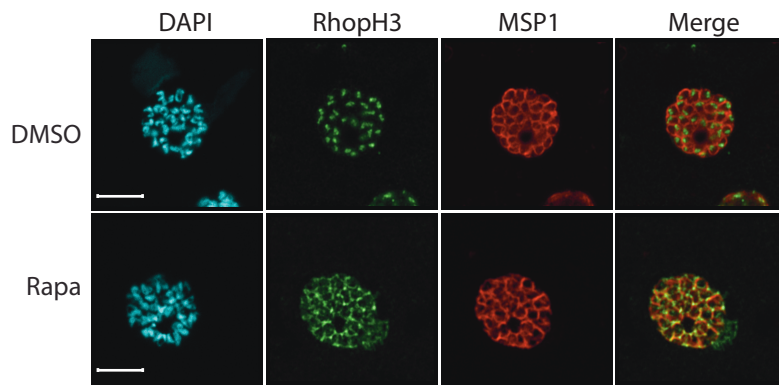


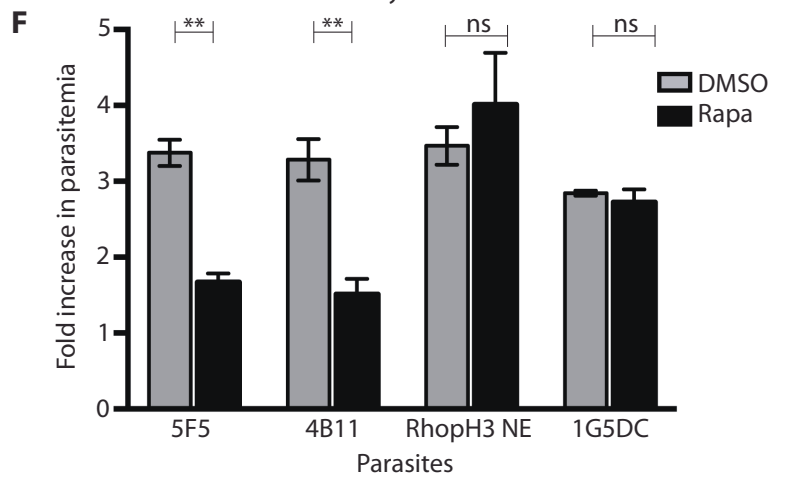
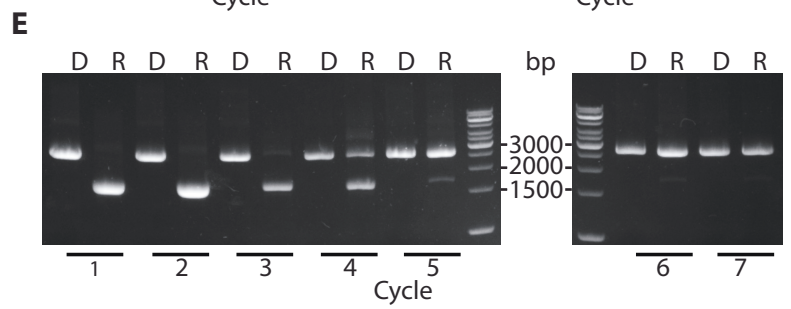
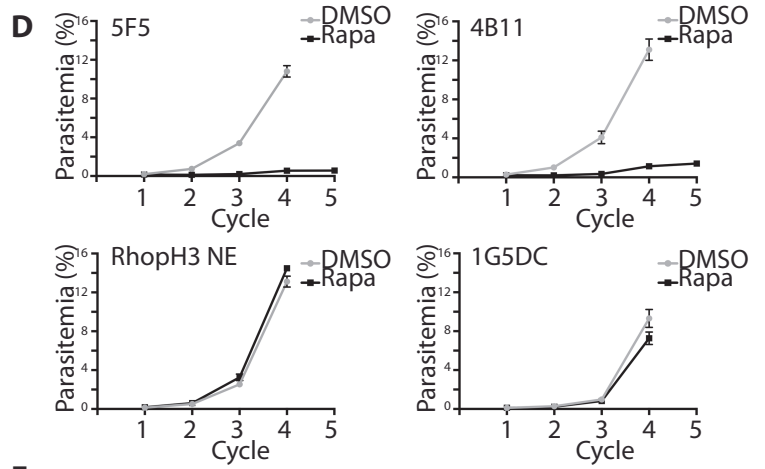
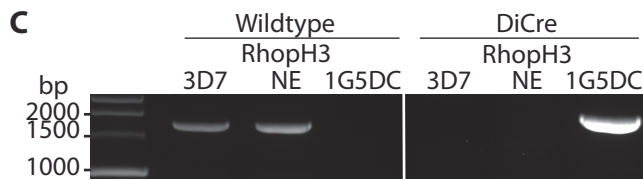
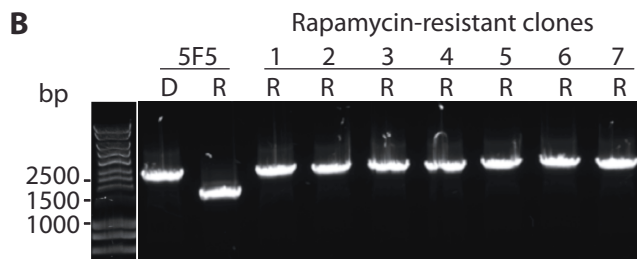
Probed: anti-RhopH3



Probed: anti-EBA175







Sherling *et al.* Figure 4

